IEEE Photonics Journal
An IEEE Photonics Society Publication

Open Access

Performance Optimization of Organic Solar Cells

Volume 6, Number 4, August 2014

Y. Q. Wong, Member, IEEE
H. Y. Wong, Senior Member, IEEE
C. S. Tan, Senior Member, IEEE
H. F. Meng

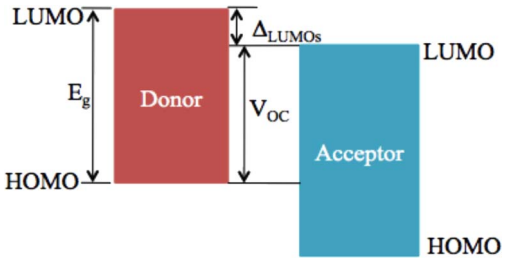

DOI: 10.1109/JPHOT.2014.2337896
1943-0655 © 2014 IEEE

IEEE photonics SOCIETY

IEEE

Performance Optimization of Organic Solar Cells

Y. Q. Wong,[1] *Member, IEEE*, H. Y. Wong,[1] *Senior Member, IEEE*, C. S. Tan,[1] *Senior Member, IEEE*, and H. F. Meng[2]

[1]Faculty of Engineering, Multimedia University, Cyberjaya 63100, Malaysia
[2]Institute of Physics, National Chiao Tung University, Hsinchu 300, Taiwan

DOI: 10.1109/JPHOT.2014.2337896

Manuscript received June 3, 2014; revised July 1, 2014; accepted July 3, 2014. Date of publication July 10, 2014; date of current version July 31, 2014. Corresponding author: Y. Q. Wong (e-mail: lana_1123@hotmail.com).

Abstract: Organic solar cells (OSCs) have been gaining great popularity in recent years due to their potentials to be low cost, lightweight, and flexible. The performance of OSCs is growing steadily, and they have achieved a power conversion efficiency close to 10% (for single-junction polymer–fullerene OSC). Although there are still limitations and challenges faced by the development of OSCs, in view of the potentials, recent studies have been focusing on the design optimization of OSC layer structure through material engineering, interfacial layer insertion, layer thickness optimization, and morphological control. In this paper, we provide a comprehensive review and detailed discussion on the optimization works and development on OSCs, with particular focus on the bulk-heterojunction (BHJ) polymer–fullerene OSCs. We also provide a summary of the performance, in a chronological order, and the future outlook of OSC.

Index Terms: Organic materials, theory and design.

1. Introduction

Solar energy is a very promising alternative energy source as it is clean and sustainable. Unlike fossil fuels, solar energy does not contribute to the degradation of our environment and it is unlimited, as the source of the energy is the Sun. However, solar energy is not widely used due to the high cost per watt delivery, attributed to the materials i.e., Silicon and the complex manufacturing methods of the first-generation inorganic-based solar cells [1]. In order to achieve a truly low cost solar technology, the materials used should be of low-cost and the manufacturing methods should be kept simple with no high temperature processes involved. As such, organic solar cells (OSCs) have been gaining popularity as they potentially achieved these and high power conversion efficiency (PCE) [2]. Moreover, OSCs can be printed from the form of solution. The developments of ink-jet printing, micro-contact printing and other soft lithography techniques made the low-cost fabrication of large-area integrated devices on both rigid and flexible substrates possible. However, to-date, the achieved PCE of OSCs is still relatively low, compared to their inorganic solar cells counterpart. This is because of their excitonic nature upon light incident, where an exciton with a small diffusion length [3]–[5] is generated instead of free charge carriers. Also, they have a relatively low number of charge carriers [6]. Thus, there is a need to enhance the PCE of OSCs. It is estimated that organic-based solar devices are required to have a PCE of 5% to 10% and a lifetime of 5 to 10 years in order to accomplish cost-efficient power generation [7].

In general, there are two types of OSCs, small-molecules and polymers, depending on the organic donor's constituent molecules. The small-molecule solar cells are mainly processed using thermal evaporation deposition in a high-vacuum environment, which is expensive. On the other hand, polymer solar cells (PSCs) are solution-processed. The process is relatively simple with low manufacturing energy and inexpensive. As such, PSCs are studied intensively. In addition to that, the implementation of C_{60} fullerene and its derivatives such as [6,6]-phenyl-C_{61}-butyric acid methyl ester (PCBM) as the organic acceptor lead to the renowned high PCE polymer-fullerene solar cells [8]. This combination of organic materials is currently dominating the field of PSCs.

As for the structure employed in PSCs, there are commonly two types, namely planar and bulk-heterojunction (BHJ). A planar cell is simply a cell with donor and acceptor materials on top of one another while BHJ is a mixture of donor and acceptor materials in a bulk device. Due to the short exciton diffusion length, the bilayer planar structure is restricted to a layer thickness of only 5–10 nm [9]. This ensures the free charge carriers are able to reach the electrodes more efficiently with lesser probability of recombinations and trapping. However, at the same time, due to its thin nature, its light absorption is also relatively lower compared to BHJ cell. On the contrary, BHJ cell can have a layer thickness of more than 10 nm. Although it has a relatively higher probability of recombinations and trapping, due to its interpenetrating network of donor and acceptor [10], its relatively higher thickness also ensures that the cell has greater light absorption and higher interfacial area for exciton dissociation. Most importantly, BHJ PSCs are also compatible with the low-cost manufacturing techniques such as inkjet printing, spin coating and roller casting [9], [11], [12]. Few years after the realization of efficient BHJ PSCs by Heeger and Friend [13], the number of scientific publications in the field rises exponentially. Promising PCEs are reported for BHJ PSCs, with values exceeding 5% [14]–[16] reported around year 2006 and with improved values exceeding 8% [11], [17]–[19] reported in recent years.

There are four processes involved in converting the sunlight to electricity in OSC, with each process characterized by an efficiency. These efficiencies are (a) light absorption efficiency, η_A (b) exciton diffusion efficiency, η_{ED} (c) charge separation efficiency, η_{CS} and (d) charge collection efficiency, η_{CC}. When the light beam passes through the transparent anode to the donor, the photon is absorbed at the donor layer (based on the generalization that the organic donor is the light-absorbing material). An electron is excited from the highest occupied molecular orbital (HOMO) to the lowest unoccupied molecular orbital (LUMO), creating a bound electron-hole pair, known as an exciton. The exciton binding energy, which is the Coulombic attraction of the bound electron-hole pair [9], is generally large (0.1–1.0 eV) and the built-in electric field strength is usually insufficient to dissociate the exciton directly [3]. As such, the dissociation occurs almost exclusively at the interface between the donor and acceptor [20], which has different electron affinities and ionization potentials [9]. Thus, after excitation, the exciton diffuses to the donor-acceptor interface. There, the excited electron is transferred to the LUMO of the acceptor, and the energy difference between the LUMOs of the donor and acceptor drives the dissociation of the exciton into free charge carriers. The free hole and electron are then collected by the anode and the cathode respectively.

The efficiencies of the four processes define the external quantum efficiency (EQE) of the solar cell [21]. It is also known as incident photon-to-current collection efficiency (IPCE), which is the number of electrons produced by a solar device for each incident photon. Meanwhile, the PCE of the solar cell is measured by the ratio of the output power (P_{out}) to the input power (P_{in}), which is governed by the open-circuit voltage (V_{OC}), the short-circuit current (J_{SC}), and the fill factor (FF) of the device [22].

$$PCE = V_{OC} \times J_{SC} \times FF/P_{in} \tag{1}$$

Various techniques are employed to enhance these parameters. They will be discussed in the following sections. This review article focuses on the performance optimization of BHJ

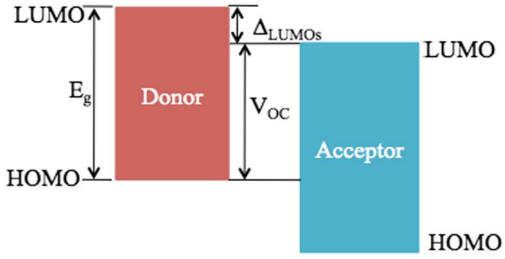

Fig. 1. Bandgap energy levels of donor and acceptor.

polymer-fullerene solar cells. We will discuss their development, on how material engineering, interfacial layer insertion, layer thickness optimization and morphological control help to enhance the PCE. All literature discussed are summarized in Table 3 in Section 2 for ease of reference. Finally, we conclude by identifying some potential areas for future development. Henceforth, the usage of the word "OSC" will mainly refer to BHJ polymer-fullerene solar cell.

2. Performance Optimization of OSC

2.1. Material Engineering

Materials play a very important role in determining the overall performance of an OSC because the properties of the materials such as molecular energy levels, bandgaps (E_g), and carrier mobilities greatly affect the devices performance.

In the early 2000s, research was extensively focused on the donor material poly(3-hexylthiophene) (P3HT) [23]–[26]. This was because P3HT has a relatively low bandgap (E_g) of around 1.9 eV, compared to 2.1 eV to 2.2 eV of similar PPV derivatives, thus covering broader spectrum absorption [9]. Increased absorption results in increased numbers of photogenerated carriers and in turn, increased number of carriers collected at the electrodes. This led to a high EQE value. P3HT is the first ever polymer that demonstrated a J_{SC} value as high as 8.7 mA/cm^2 [28]. Also, P3HT exhibits high hole mobility of up to 0.1 cm^2/Vs [29], which allows the incorporation of thicker active layers for better light absorption and efficient charge transport to the electrodes. Moreover, thermal annealing of the P3HT:PCBM blend [24], which appears to be a crucial post-treatment for the device to achieve high PCE is identified. These positive findings encourage even more researchers to study this blend of materials. However, it was soon realized that this blend has reached its maximum PCE limit of around 5% where it could not go beyond this value. This restriction is due to the high-lying HOMO of P3HT (4.9 eV) [30], which gives a maximum V_{OC} of only around 0.6 V. Hence, many researchers begin to search for new methods to increase V_{OC} through material engineering.

V_{OC} is proportional to the molecular energy level difference between the HOMO of the donor and the LUMO of the acceptor [16], [31] (see Fig. 1). This has been proven experimentally [3], [32], [33], and the relationship can be represented in

$$V_{OC} = e^{-1}x\left(|E_{HOMO}^{Donor}| - |E_{LUMO}^{Acceptor}|\right) - 0.3\ eV \tag{2}$$

where e is the elementary charge, with the general value of 1.6×10^{-19} C, E is the energy level, and 0.3 eV is an empirical value for efficient charge separation [34]. Thus, an acceptor with a high-lying LUMO and/or a donor with a low-lying HOMO is essential to achieve a high V_{OC}.

Utilizing less electron-rich groups [22], [35]–[37] such as fluorine and carbazole helps to lower the HOMO level of the material. It was demonstrated that through this method a high V_{OC} device was indeed obtained. Poly-9,9-dioctylfluorene, 4-7-di-2-thienyl-2,1,3-benzothiadiazole

TABLE 1

Properties and device characteristics of the polymer

Polymer	HOMO (eV)	LUMO (eV)	V_{OC} (V)	Ref
PBDTTT-E	5.01	3.24	0.62	[43]
PTB4	5.12	3.31	0.76	[17]
PBDTTT-C	5.12	3.55	0.70	[44]
PBDTTT-S	5.12	2.81	0.76	[45]
PBDTTT-CF	5.22	3.45	0.76	[43]
PFO-DBT	5.40	3.53	0.95	[22]
PCDTBT	5.50	3.60	0.88	[38]
APFO-15	6.30	3.6	1.0	[36]

*Arrange in increasing value of HOMO

(PFO-DBT) with a HOMO of 5.4 eV reported a V_{OC} of 0.95 V [22]. Another polyfluorene (PF) copolymer poly[2,7-(9,9-dioctylfluoren)-alt-5,5-(5′,8′-di-2-thienyl-(2′,3′-bis-(3″-octyloxyphenyl)-quinoxaline))] (APFO-15) is synthesized with donor-acceptor-donor structure in between the fluorine units [36]. Its HOMO is 6.3 eV. The best performing device for this material blended with PCBM achieved a V_{OC} of 1.0 V. Nevertheless, polyfluorene has relatively low hole mobility and this results in PCEs of only around 3%. On the other hand, poly(N-vinylcarbazole) (PVK) is well-known to be an excellent photoconductor [35]. Its derivative, poly[N-9′-heptadecanyl-2,7-carbazole-alt-5,5-(4′,7′-di-2-thienyl-2′,1′,3′-benzothia-diazole)] (PCDTBT) has a relatively low-lying HOMO of 5.5 eV [38]. The device using PCDTBT as the donor gives a V_{OC} in excess of 0.8 eV. In addition, this polymer has extended red-absorption, which leads to a greater coverage of the solar spectrum. After optimization, the OSC utilizing PCDTBT as its donor achieved PCE of more than 5% [4], [39]– [41].

Modifying the side groups of the polymer with different electron-withdrawing effect also results in different molecular energy level polymers [42]. Using poly[4,8-bis-substituted-benzo[1,2-b:4,5-b0] dithiophene-2,6-diyl-alt-4-substituted-thieno[3,4-b]thio-phene-2,6-diyl] (PBDTTT-based) polymer as an example, higher V_{OC} devices are progressively achieved by attaching the side groups with increasing electron-withdrawing effect, which are ester [43], carbonyl [44], carbonyl and fluorine [43], and sulfonyl [45] respectively.

The polymer based on alternating ester substituted thieno[3,4-b]thiophene and benzodithiophene units (PBDTTT-E) has a HOMO and LUMO of 5.01 eV and 3.24 eV respectively. This polymer has a V_{OC} of 0.62 V and a high J_{SC} of 13.2 mA/cm^2 [43]. To further lower its HOMO level, fluorine was introduced into the thieno[3,4-b]thiophene unit to produce a polymer known as PTB4. It has a HOMO of 5.12 eV and this gives an enhanced V_{OC} of 0.76 V [17]. Aside from adding fluorine, the V_{OC} could also be enhanced by removing the oxygen atom from the ester group in the thieno[3,4-b]thiophene unit and replaced it with ketone to produce PBDTTT-C [44]. PBDTTT-C has a relatively low HOMO and LUMO of 5.12 eV and 3.55 eV. The device based on PBDTTT-C showed promising results with $V_{OC} = 0.70V$, $J_{SC} = 14.7mA/cm^2$, $FF = 0.64$ and $PCE = 6.58\%$. To further lower the HOMO level, having more than one electron-withdrawing group in the PBDTTT-based polymer has also been proven to be an effective method [43]. Introducing an additional fluorine to the thieno[3,4-b]thiophene unit of PBDTTT-C polymer resulted in PBDTTT-CF with a HOMO of 5.22 eV and a V_{OC} of 0.76 V. Thus far, fluorine has been frequently used to lower both the HOMO and LUMO energy levels of polymer. However, the high cost and tedious synthesis of fluorinated monomer encouraged the development of another PBDTTT-based polymer with sulfonyl as the electron-withdrawing side group [45]. PBDTTT-S has a HOMO level of 5.12 eV and demonstrated broad absorption. The device based on this donor polymer achieved a V_{OC} of 0.76 V and a PCE of 6.22%, indicating that sulfonyl group is a promising candidate for applications in PSCs. Table 1 shows the polymers with their HOMO/LUMO values and the V_{OC} achieved.

J_{SC} is also one of the key parameters that influences the performance of OSCs. It is an integral of the product between the cell responsitivity and the incident solar spectral irradiance [31],

as represented by

$$J_{sc} = \frac{hc}{q} \int_{\lambda_1}^{\lambda_2} \frac{P_{AM1.5G}(\lambda) xEQE(\lambda) d\lambda}{\lambda} \tag{3}$$

where h is the Plank's constant $(6.626 \times 10^{-34}$ Js or 4.136×10^{-15} eVs), c is the speed of light in vacuum $(3 \times 10^8$ ms$^{-1})$, q is the elementary charge (same with e mentioned in equation (2)), λ_1 and λ_2 are the respective minimum and maximum wavelength of the active spectrum being considered and $P_{AM1.5G}$ is the Air Mass 1.5 given by the ASTM Standard G159 [46].

The cell responsitivity is related to the E_g of the material. Only photons with an energy value larger than the material E_g are being absorbed. The larger the E_g, the poorer the spectral overlap with the photon flux from the sun [9]. For example, the material P3HT has a E_g of around 1.9 eV whereas the maximum photon flux of the solar spectrum is at around 1.6 to 1.8 eV [47]. Their differences result in a mismatch of the material absorption with the solar spectrum. This is another reason the solar device using P3HT as the donor could not exceed the PCE of 5%.

Ideally a donor material should have a relatively small E_g value, around 1.3–1.5 eV so that it covers the absorption for higher wavelength range. Low-bandgap polymer red-shifts the absorption to include absorption at longer wavelength. This may potentially lead to improvement in J_{SC} if other properties of the material such as charge mobility and energy levels are favorable [47].

There are many ways to attain a low-bandgap polymer and the most common method is by designing an alternating donor-acceptor structure [48]–[50]. The result is a polymer with a higher HOMO and lower LUMO. Some examples of these alternating donor-acceptor low-bandgap polymers are polythiophene-benzothiadiazole copolymer (PTPTB) $(E_g = 1.6$ eV) [51]–[54], polyfluorene-benzothiadioazole copolymer (PFDTBT) $(E_g = 1.9$eV) [55], [56] and poly[2, 6-(4,4-bis-(2-ethylhexyl)-4H-cyclopenta[2,1-b;3,4-b']dithiophene)-alt-4,7-(2,1,3-benzothiadiazole)] (PCPDTBT) $(E_g = 1.5$ eV) [15], [47]. PCPDTBT is one of the most successful examples of low-bandgap polymers. Its bandgap is the lowest compared to the other examples presented and its absorption extends up to 900 nm. It shows improved charge-transport properties, fitting electronic energy levels and good processability [47]. When paired with PCBM, the device delivered a high J_{SC} of 9 mA/cm^2 [47] compared to PTPTB with 3.1 mA/cm^2 [54] and PFDTBT with 7.7 mA/cm^2 [42]. Most of the polymers listed in Table 1 are also low-bandgap polymers with J_{SC} values above 10 mA/cm^2 [17], [38], [43], [44].

Low-bandgap polymer can also be obtained by reducing the LUMO level of the polymer and keeping the HOMO level unchanged. One example material is the regioregular poly(3-hexylselenophene) (P3HS) [57], a selenium analogue of P3HT. P3HS has a smaller bandgap of 1.6 eV, compared to P3HT with a bandgap of 1.9 eV. Hence, P3HS:PCBM has better absorption at the longer wavelength region of the solar spectrum due to its extended spectral sensitivity. However, since their HOMOs are similar, the device made from P3HS and P3HT each has a similar V_{OC} value of around 0.5 V.

A higher J_{SC} can also be achieved by using another C_{60} derivative as the acceptor. The blend of PCPDTBT with [6,6]phenyl-C_{71}-butyric acid methyl ester $(PC_{70}BM)$ gave a higher J_{SC} of 11 mA/cm^2 compared to a J_{SC} of 9 mA/cm^2 when pairing with PCBM [47]. The reason for the higher J_{SC} was because this acceptor helps to extend the effective spectral range for the photocurrent [58], as shown in Fig. 2. The additional contribution from $PC_{70}BM$ at around 500 nm accounts for the enhanced EQE.

A novel donor polymer poly[[4,8-bis [(2-ethylhexyl)oxy]benzo[1,2-b:4,5-b']dithiophene-2,6-diyl] [3-fluoro-2-[(2-ethylhexyl)carbonyl]thieno[3,4-b]thiophenediyl]] (PTB7) with a good solubility in organic solvents, a high hole mobility of $5.8 \times 10 - 4$ cm^{2}V^{-1}s^{-1} and a strong absorption from 550 nm to 750 nm was also paired with $PC_{70}BM$ to achieve a better coverage of the solar spectrum. PTB7 has relatively weak absorption from 300 nm to 500 nm. By blending with $PC_{70}BM$, the resulting device had strong absorption from 300 nm to about 800 nm, delivering a J_{SC} of 13.56 mA/cm^2 [11].

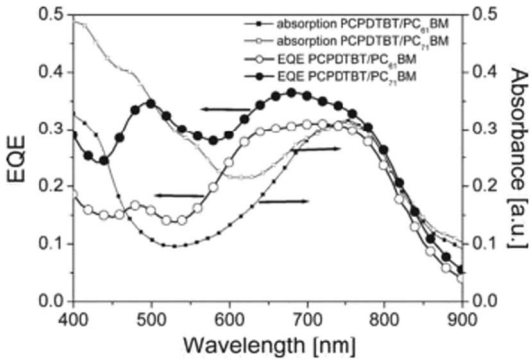

Fig. 2. EQE and absorption spectra of PCPDTBT:PCBM blend and PCPDTBT:$PC_{70}BM$ blend [47].

It is noteworthy that the enhancement of V_{OC} and J_{SC} in terms of modifying molecular energy levels and E_g are contradicting with each other. To achieve a high V_{OC}, a material with a high-lying acceptor LUMO and/or a low-lying donor HOMO is required. As for high J_{SC}, a low-bandgap material is needed, where it normally has a high-lying donor HOMO. It poses a challenge to improve both the V_{OC} and the J_{SC} simultaneously. However, in recent years, researchers discover that structural fine-tuning is able to improve both these parameters simultaneously.

PBDTTT is structurally modified to two different polymers: thienyl-substituted 4,8-bis(5-(2-ethyl-hexyl)-thiophene-2-yl) (BDT) with alkoxycarbonyl-substituted thieno[3,4-b]thiophene (TT-E) and thienyl-substituted BDT with alkylcarbonyl-substituted thieno-[3,4-b]thiophene (TT-C). They are also known as PBDTTT-E-T and PBDTTT-C-T respectively. Compared with their alkoxy-substituted BDT (BDT-O) analogues, PBDTTT-E and PBDTTT-C, thienyl-substituted BDTs shows improved hole mobilities, broadened absorption, and lower HOMO and LUMO. These lead to higher J_{SC} and V_{OC} values, which result in a significant increase in PCE values. For PBDTTT-E-T, the PCE increased by approximately 50% to 6.21% relative to PBDTTT-E. As for PBDTTT-C-T, the PCE increased by approximately 20% to 7.59%, relative to PBDTTT-C [59].

Another conjugated polymer, combining BDT and thieno[3,4-c]pyrrole-4,6-dione (TPD) units also demonstrated great potential for application in OSC. TPD unit has a relatively strong electron-withdrawing effect, which leads to a low-lying HOMO and LUMO (high V_{OC}) and improved solubility. Without any postproduction treatment, this PBDTTPD blended with $PC_{70}BM$ exhibited $V_{OC} = 0.85$ V, $J_{SC} = 9.81$ mA/cm^2, FF $= 0.66$ and PCE $= 5.5\%$ [60].

Beside V_{OC} and J_{SC}, the molecular energy level of the materials also affects the η_{CS}. The LUMO differences between the donor and acceptor drive the exciton dissociation at the donor-acceptor interface [20]. For devices in which the acceptor absorbs a significant amount of photon, the same concept applies, but in terms of the HOMO differences and this is discussed elsewhere [61]. These energy level differences are necessary for the initial electron transfer from the donor to the acceptor.

Generally, the minimum LUMO difference between the donor and acceptor is 0.3 eV and this is able to split the exciton into free charge carriers. A much higher LUMO energy difference than the exciton binding energy is not beneficial to this dissociation process as it results in wasted energy [62].

This information can serve as an approximate guidance of selecting the active materials with appropriate molecular energy levels and bandgaps in order to have an optimum value of V_{OC} and J_{SC}. In the next section, we will discuss how the interfacial layer plays a role in optimizing the performance of an OSC.

2.2. Interfacial Layer Insertion

Efficient charge collection at the electrodes is very important to ensure that the photogenerated free charge carriers are collected at their respective electrodes and are converted to

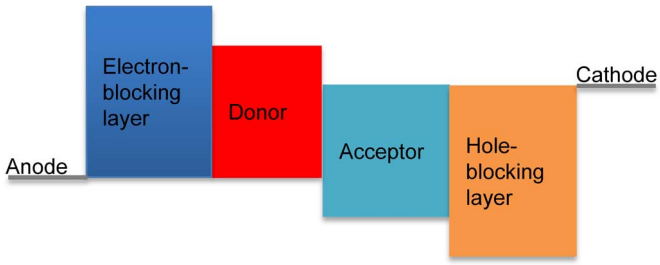

Fig. 3. Relative molecular energy levels and work functions of the materials in an OSC device.

produce electricity. Inserting interfacial layers between the electrodes and the active layer helps to minimize the free charge carrier recombination [63], spatially redistribute light intensity in the device [13] and prevent current leakage [64]. There are two types of interfacial layers. The interfacial layer between the anode and the active layer is commonly referred to as the electron-blocking layer or hole-transport layer, whereas the interfacial layer between the cathode and the active layer is commonly known as hole-blocking layer or electron-transport layer. This is illustrated in Fig. 3.

Holes are attracted to the anode and electrons are attracted to the cathode due to a built-in electric field, which arises from the work function difference between the electrodes. Simultaneously, there is a competing cell voltage that opposes the built-in field [20]. Thus, regardless of the field strength, the electron-blocking layer is designed to prevent electron leakage, where the electrons in the acceptor phase are not able to flow into the anode. At the same time, the electron-blocking layer facilitates hole extraction at the anode. This is achieved by inserting an interfacial layer with a sufficiently high LUMO compared to the LUMO of the donor, and a matching HOMO with the donor and the work function of the anode.

As for the hole-blocking layer, it is designed to prevent the holes in the donor phase to flow into the cathode. It also facilitates electron extraction at the cathode [34]. A suitable hole-blocking layer is one having a sufficiently low HOMO compared to the HOMO of the acceptor, and a matching LUMO with the acceptor and the work function of the cathode (refer to Fig. 3). Choosing a suitable interfacial layer with appropriate energy level can increase the charge collection efficiency (η_{CC}).

Poly(3,4-ethylenedioxy thiophene)/poly(styrene sulfonic acid (PEDOT:PSS) is the most commonly used electron-blocking layer in OSC. When incorporated into P3HT:PCBM blend, this device exhibited PCE of more than 3% [13], [65], with enhancement of around 60%, compared to the device without an electron-blocking layer. PEDOT:PSS helps to improve holes extraction [66], [67], establish better contact between the anode and active layer [68], planarizes the surface roughness of ITO [69], [70] and inhibits the dewetting of the overlying organic layers [71].

Despite the advantages offered by PEDOT:PSS, there are many disadvantages as well, such as moisture absorption from air that undergoes a migration into the active layer, device performance degradation over time [72], highly acidic nature with pH level around [73]–[76], and large microstructural and electrical inhomogeneities with morphology and conductivity varying by orders of magnitude over different film regions [77].

Since the benefits of having interfacial layer supersede the aforementioned difficulties, another type of electron-blocking layer, using transition metal oxide, was proposed [65] as an alternative. Two types of transition metal oxides were investigated, vanadium oxide (V_2O_5) and molybdenum oxide (MoO_3) and their performances were compared against that of PEDOT:PSS. The device tested was of the structure ITO/electron-blocking layer/P3HT:PCBM/Ca/Al. The results are shown in Table 2 and they are illustrated in Fig. 4.

After inserting an electron-blocking layer, all the photovoltaic (PV) parameters, J_{SC}, V_{OC}, FF, and PCE were improved. Although the PCE for the device using V_2O_5 as electron-blocking layer was slightly lesser compared with the device using PEDOT:PSS, metal oxide V_2O_5 is a suitable substitute for PEDOT:PSS. This is because V_2O_5 effectively blocks electrons from entering the

TABLE 2

Summary of device performance using different electron-blocking layer

Electron-blocking Layer	V_{OC} (V)	J_{SC} (mA/cm^2)	FF	PCE (%)
Without electron-blocking layer	0.49	7.82	0.511	1.96
PEDOT:PSS	0.59	8.95	0.596	3.18
V_2O_5	0.59	8.83	0.591	3.10
MoO_3	0.60	8.94	0.619	3.33

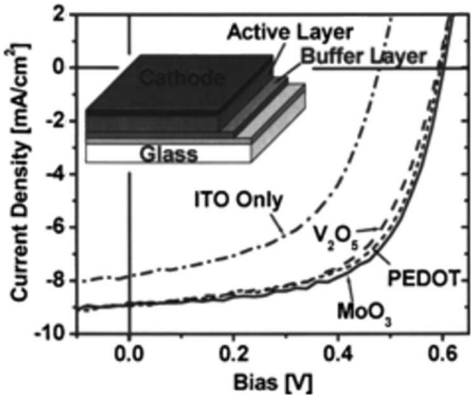

Fig. 4. J-V characteristics for four devices (ITO only, ITO with PEDOT:PSS, ITO with V_2O_5 and ITO with MoO_3) under illumination [65].

anode and it does not have the disadvantages as observed in PEDOT:PSS. On the other hand, the device using MoO_3 exhibited the best performance in this work, with 70% enhancement in PCE, compared with the device without an electron-blocking layer.

Since MoO_3 showed the best enhancement compared with PEDOT:PSS and V_2O_5, it was incorporated into PCDTBT:PC_{70}BM blend. Results showed that the charge extraction and the formation of ohmic contact were improved [38]. These were due to the higher work function of MoO_3, around 5.6 eV, which resembles a closer match to the HOMO of PCDTBT (5.5 eV) compared to PEDOT:PSS with a work function of 5.0 eV [78]. The air stability of the device was also improved, where the PCE of unencapsulated device maintained above half of the original value even after storage in air for 720 h. Comparatively, the device fabricated with PEDOT:PSS showed rapid degradation after the same storage time.

Also, the device with MoO_3 exhibited a higher EQE at wavelengths between 350 nm and 500 nm as compared to the control device. The MoO_3 films consisted of small islands that extended the contact area between the active layer and the interfacial layer. This encouraged efficient holes collection. Although the increment in thickness led to reduction in J_{SC}, the reduction is not as bad as compared to the device using PEDOT:PSS as interfacial layer. The device fabricated with MoO_3 allowed the PCDTBT:PC_{70}BM structure achieved a relatively high PCE even when the active layer had a thickness of up to 200 nm [38]. It showed $J_{SC} = 10.88$ mA/cm^2, $V_{OC} = 0.89$ V, FF $= 0.67$, PCE $= 6.5\%$ whereas for the control device, without MoO_3, it showed $J_{SC} = 10.11$ mA/cm^2, $V_{OC} = 0.88$ V, FF $= 0.67$ and PCE $= 5.95\%$ [38]. The enhancement in J_{SC} was mainly attributed to the favorable redistribution of light intensity within the active layer.

Another example of electron-blocking layer made of transition metal oxide is nickel oxide (NiO). NiO is a cubic wide band-gap semiconductor that is transparent as very thin layers and is

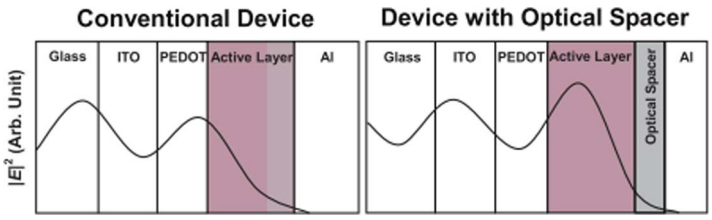

Fig. 5. Schematic representation of the spatial distribution of the squared optical electric-field strength $|E^2|$ inside the devices for (a) conventional device without an optical spacer [82] and (b) device with optical spacer [13].

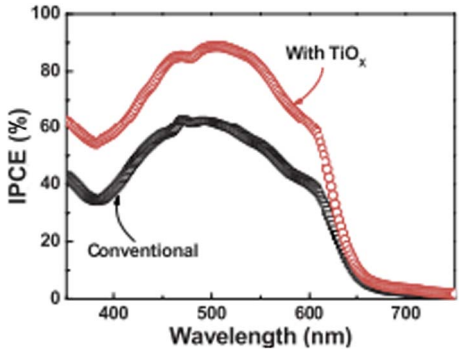

Fig. 6. Incident monochromatic photon-to-current collection efficiency spectra for conventional device and device with the TiO_X optical spacer [13].

a p-type material that facilitates hole conduction. Irwin *et al.* [64] investigated its usage in preventing current leakage and consequent counterdiode formation [79]. The results showed that by using NiO, the PCE was enhanced significantly from 2.87% to 5.16%.

However, the metal oxide interfacial layers may contribute to series resistance of the device and higher thickness may result in lower current, which decrease the FF of the device. With an optimized thickness of the oxide layer, they form a uniform contact with the polymer to reduce current leakage, giving improvement in both J_{SC} and FF. In addition, note that although all the interfacial layers have different work functions ($V_2O_5 = 4.7$ eV, $MoO_3 = 5.3$ eV, PEDOT:PSS $=$ 5.2 eV), the V_{OC} is not altered as much. This indicates that the V_{OC} is independent of the work function of the anode material [65].

On the other hand, Kim *et al.* [13] investigated on the solution-based titanium oxide interfacial layer as an optical spacer. It was inserted between the active layer and the metal back electrode (cathode). The optical interference between the incident and back-reflected light in a solar cell results in a low squared optical electric-field strength in the active layer [80]–[82], as shown in Fig. 5 [13], [82], and hence, the low photogeneration of carriers. The optical spacer spatially redistributes the light intensity in the device.

Some of the criteria of an optical spacer are: a good acceptor, an electron-transport material with a LUMO lower than the LUMO of C_{60} but at the same time, higher or close to the Fermi energy of the metal back electrode. Also, the optical spacer must be transparent to light with wavelengths within the solar spectrum. Titanium oxide (TiO_X) is a suitable candidate because it is an electron acceptor and a transport material, as confirmed by its extensive use in dye-sensitized cells [83], [84], hybrid polymer/TiO_2 cells [85]–[87], and multilayer Cu-phthalocyanine/dye/TiO2 cells [82], [88].

The TiO_X layer was fabricated on top of the P3HT:PCBM active layer using solution-based sol-gel process. As shown in Fig. 6, an IPCE enhancement of around 40% at 500 nm was observed. The enhancement was attributed to the increased absorption in the BHJ layer, due to the spatial redistribution by the TiO_X. Under AM1.5 illumination (90 mW/cm2), the PV data

obtained for the device with and without the TiO_X optical spacer were $J_{SC} = 11.1$ mA/cm^2, $V_{OC} = 0.61$ V, FF $= 0.66$, PCE $= 5\%$, and $J_{SC} = 7.5$ mA/cm^2, $V_{OC} = 0.51$ V, FF $= 0.54$, PCE $= 2.3\%$, respectively. The increase in the device PCE was attributed to the significant increase in J_{SC}, consistent with the IPCE measurements.

TiO_X was also applied to PCDTBT:PC_{70}BM blend [39]. The redistribution of light intensity within the blend, the matching of the bottom of the conduction band of TiO_X with the LUMO of PC_{70}BM, and the hole-blocking function enable high electron collection efficiency. Experiments were done to compare the absorption between the device of the structure ITO/PEDOT:PSS/PCDTBT:PC_{70}BM/Al with and without TiO_X. The device with the TiO_X layer exhibited higher absorption and thus, the device demonstrated a higher EQE as well. Together with an optimized choice of solvent (in this case, dichlorobenzene) and a blend ratio of 1 : 4, this device exhibited the PV characteristics $J_{SC} = 10.6$ mA/cm^2, $V_{OC} = 0.88$ V, FF $= 0.66$, and PCE $= 6.1\%$.

However, the thickness of the TiO_X optical spacer is governed by the thickness of other layers such as the ITO, PEDOT:PSS and BHJ layer as well [89]. It is cumbersome and costly to control and monitor every optical thin film in the OSC production process. As such, an alternative to TiO_X, Lithium Floride (LiF) can be used. LiF forms an effective interfacial dipole between aluminium (Al) and an organic semiconductor, which reduces the work function of Al [90]. Besides, LiF also helps to improve the formation of an ohmic contact with the active layers, resulting in enhanced FF and V_{OC}. With an optimum thickness of LiF, in the range of 0.8 to 1.0 nm, the PCE of the device reached 5.6% [4].

From the examples above, the importance of having interfacial layers in OSC is highlighted. Majority of the organic-based solar devices consist of at least one interfacial layer in order to achieve higher performance. In the next section, we will discuss on the variation of the thickness of the interfacial layers and/or thickness of the active layers to improve the absorption efficiency (η_A), which is one of the processes involved in converting sunlight to electricity.

2.3. Layer Thickness Optimization

Absorption efficiency (η_A) is related closely to absorption coefficient (α). α depends on the material and on the wavelength of light absorbed. Different semiconductor materials have different α and they determine how far the light with a particular wavelength can travel into a material before it is absorbed. Light with an energy value below the E_g of the material is not absorbed because the energy is not sufficient to excite the electron.

Most of the organic materials have a E_g of around 2 eV [3]. This is relatively high compared to inorganic materials such as silicon with a E_g value of 1.1 eV [91]. This results in poor harvesting of the solar spectrum. In addition to that, commonly, a thick cell is required to absorb most of the incident sunlight but a thick cell is expensive as it uses more materials and the path of the free charge carriers travelling to the electrodes is long. Competing processes such as back electron transfer or recombination eventually results in some losses [92]. Due to the low charge mobility (10^{-7} cm^2/Vs to 10^{-1} cm^2/Vs) [93] of OSC, the thickness must be controlled to ensure the free charge carriers reach their respective electrodes before they recombine.

Fortunately, most organic materials have high absorption coefficients of more than 10^5 cm^{-1} [92]. Using (4) to calculate, a 100 nm cell is sufficient for the light to penetrate into the cell and be absorbed by a factor of 1/e [94]. Therefore, the active layer thickness is typically around 100 nm, which is also chosen based on convenience and empirical results [95]

$$d = \frac{1}{\alpha}. \tag{4}$$

The correlation between the thickness and the performance of a device was investigated by Moon *et al.* [41]. The thickness of the active layer PCDTBT:PC_{70}BM was increased from 70 nm to 200 nm. It was observed that the FF of the device decreased significantly and the series resistance almost increased twice as much. The decrease in FF was attributed to the carrier

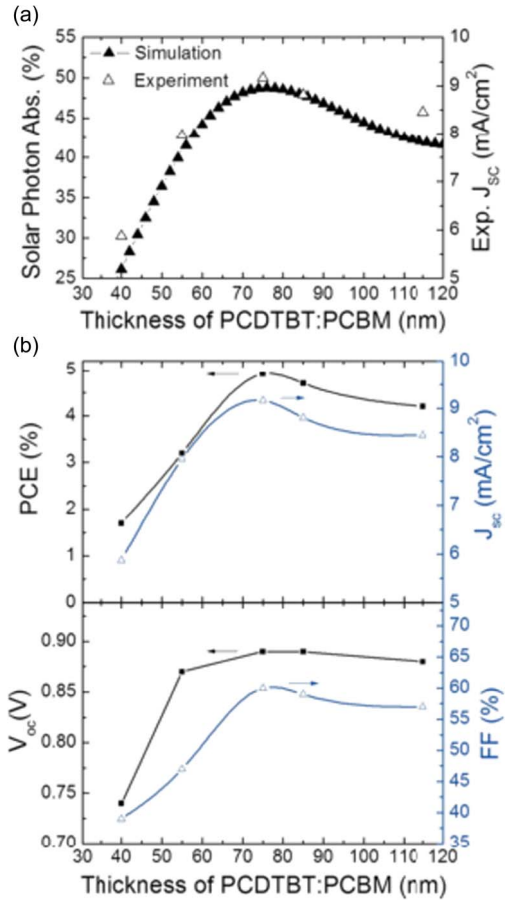

Fig. 7. Simulated solar photon absorption in the active layer of a solar cell and experimental JSC as a function of the active layer thickness. (b) Experimental thickness dependence of V_{OC}, J_{SC}, and FF [40].

recombination. Thus, the device performance was degraded when the active layer thickness was increased. The PV characteristics of the device with 70 nm active layer were $J_{SC} = 11.32$ mA/cm^2, $V_{OC} = 0.88$ V, FF = 0.69, PCE = 6.9% while the PV characteristics of the device with 200 nm active layer were $J_{SC} = 12.09$ mA/cm^2, $V_{OC} = 0.85$ V, FF = 0.53, PCE = 5.4%.

Chu *et al.* [40] attempted to maximize the solar absorption in the active layer by optimizing both the thickness of the hole extraction layer (PEDOT:PSS) and the active layer (PCDTBT: PCBM). The simulation results and experimental results were in good agreement that the optimum thickness of the active layer for the structure ITO(150 nm)/PEDOT:PSS(50 nm)/PCDTBT: PCBM(x nm)/LiF/Al was x = 75 nm, as shown in Fig. 7.

By reducing the thickness of PEDOT:PSS layer from 50 nm to 30 nm, the absorption of the active layer was further enhanced, as shown in Fig. 8. The change in the thickness of PEDOT: PSS affected the optimal thickness of the active layer as well. The optimum thickness of the active layer became 83 nm. Thus, the device ITO(150 nm)/ PEDOT:PSS (30 nm)/PCDTBT: PCBM (83 nm)/LiF/Al exhibited $J_{SC} = 9.5$ mA/cm^2, $V_{OC} = 0.91$ V, FF = 0.6, and PCE = 5.2%. The photocurrent and the FF were improved. It is noteworthy that they did not use optical spacer between the active layer and the cathode. The group asserted that if the layer thickness is already optimized, the addition of an optical spacer brings no optical benefit.

However, it was reported by Moulé *et al.* [95] that for the material with higher mobility such as P3HT ($\sim 10^{-4}$ cm^2/Vs) compared to poly(2-methoxy-5-(3′,7′-dimethyloctyloxy)-p-phenylenevinylene) (OC_1C_{10}) ($\sim 10^{-5}$ cm^2/Vs), the device would have a maximum PCE when

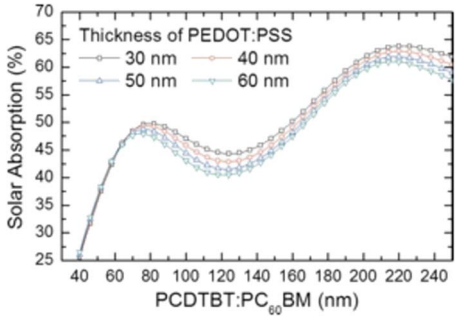

Fig. 8. Simulated solar photon absorption vs active layer thickness for different PEDOT:PSS thickness [40].

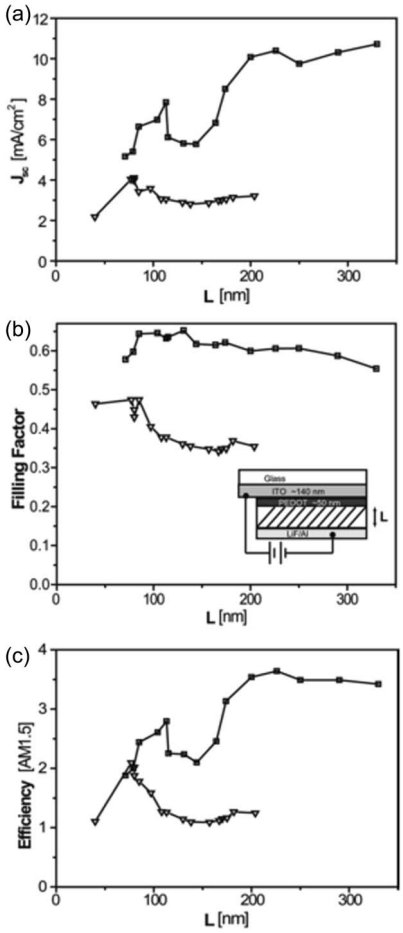

Fig. 9. Thickness dependence of (a) J_{SC}, (b) FF, and (c) PCE for (50%:50%) P3HT:PCBM (squares) and (20%:80%) OC_1C_{10}-PPV:PCBM (triangles) PV devices illuminated by AM1.5 source at 100 mW/cm^2 intensity. Inset in (b) is a schematic of the device [95].

the active layer thickness exceeds 100 nm. A series of P3HT:PCBM and OC_1C_{10}:PCBM devices with different active layer thicknesses, from as low as 50 nm to as high as 300 nm, and different donor-acceptor concentration ratios were fabricated. This was to study the effect of active layer thicknesses and concentration ratios have on J_{SC}, IPCE and PCE of OSCs. The results are shown in Fig. 9.

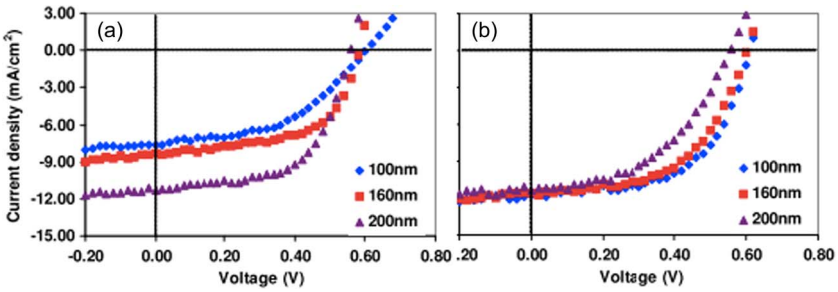

Fig. 10. Light I-V curves for P3HT:PCBM heterojunction photovoltaic cells with different active layer thickness as marked in the figure. (a) Solvent annealing only and (b) solvent/thermal annealing [96].

For P3HT:PCBM, it demonstrated a maximum PCE of 3.7% when the active layer was 225 nm and the donor-acceptor concentration ratio was 50 : 50. As for OC_1C_{10}:PCBM, it showed a maximum PCE of 2.1% when the active layer was 80 nm and the ratio was 20 : 80. By comparing the data between J_{SC} and IPCE, it was confirmed that the reductions in J_{SC} were attributed to the interference effects between the incident light and the light reflected from the back Al cathode. However, fitting of the IPCE in electrical modeling would require the optical intensity distribution in the active layer and the light absorption. In addition, the group showed that for thicker samples, a higher J_{SC} and PCE were obtained when a higher concentration of PCBM was used. For example, a P3HT:PCBM device with a thickness of 105 nm had its maximum J_{SC} when the PCBM concentration was 40%. Whereas for a P3HT:PCBM device with a thickness of 215 nm, it showed a maximum J_{SC} when the PCBM concentration was higher at 50%. In thinner device, a lower concentration of PCBM (40%) but higher concentration of P3HT (60%) resulted in increased absorption and thus increased charge generation per thickness. For thicker device, which had lowered absorption due to the higher concentration of PCBM (50%), maximum J_{SC} was attributed to the enhanced probability of exciton dissociation and decreased recombination of nongeminate charge pairs. Thus, the active layer thickness could exceed 100 nm but for each thickness, an optimum donor-acceptor concentration ratio that balances the charge generation and charge dissociation has to be found.

The active layer thickness is also found to influence the morphology and the performance of OSC when the device was subjected to post-production treatment. It is shown that upon device annealing, there is a change in the performance that is correlated to the active layer thickness. At some critical thickness, the effect of thermal annealing became negative. The microstructure and polymer ordering in the active layer are critical to the device performance and favorable morphology is more efficiently achieved in thinner film that is thermally annealed.

Results by Zhao *et al.* [96] showed that for the three sets of P3HT:PCBM devices with different thicknesses (100 nm, 160 nm, and 200 nm), initially, after solvent annealing, the thickest device (200 nm) gave the best performance [as shown in Fig. 10(a)]. However, after thermal annealing, the thinnest device (100 nm) showed the best performance [in Fig. 10(b)]. During solvent annealing, it triggered the self-assembly of P3HT molecular chains. In thinner film, since most of the solvent was already evaporated during the spin-coating process, the P3HT chains was in a more rigid phase and little solvent was left during the solvent annealing step. When subjected to thermal annealing, improved diffusion, aggregation of PCBM clusters and polymer ordering were observed and brought about the performance enhancement. On the other hand, thicker film was generally wet even after spin-coating and P3HT molecules were free to align themselves and respond dramatically to solvent annealing. However, after thermal annealing, the networking previously developed was destroyed by thermal stress. This effect exceeded the improved charge transport in the active layer effect brought about by thermal annealing, hence resulted in net performance degradation. Disregarding the cost, if the same polymer ordering, corresponding charge carrier mobility and networking in thin film could be realized in thicker

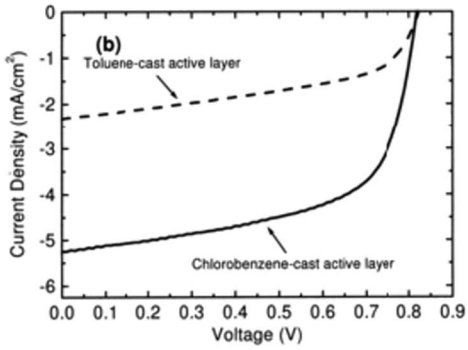

Fig. 11. Graph of current density versus voltage for device spin coated from toluene solution (dashed line) and from chlorobenzene solution (solid line) under AM1.5 illumination with intensity of 80 mW/cm^2 [98].

film, the thickness limitation of OSCs could be overcome and thicker film with enhanced absorption could be utilized to produce higher performance devices.

2.4. Morphological Control

Morphology has a big influence on the performance of OSCs as the number of factors affecting the morphology is immense and is specific to the polymer-fullerene pair used. The factors are categorized into two types, intrinsic and extrinsic. Intrinsic factors are those inherent to the donor and polymer such as the crystallinity, and the fundamental interaction between them such as relative miscibility. Extrinsic factors include all the external influences associated with device fabrication such as choice of solvents, blend ratio of donor to acceptor and deposition technique [9].

Of these intrinsic and extrinsic factors, three major factors [4] concerning the morphology of OSCs are: (a) choice of solvents, (b) blend ratio of donor to acceptor, and (c) thermal annealing. For choice of solvents, the solvents used affect the size and number of BHJ crystalline domains. As for blend ratio, it affects the formation of bicontinuous interpenetrating donor-acceptor networks. This factor addresses the issue of having charge-traps sites leading to current leakage when the free charge carriers are not collected at their respective electrodes [23], [97]. For thermal annealing, it helps in controlling the phase separation of the donor-acceptor interpenetrating network in the BHJ structure. Since the exciton diffusion length is generally less than 10 nm [3]–[5], the phase separation must be less than 20 nm. The intimate mixing of the donor and acceptor ensures that the donor-acceptor interface is within a distance less than the exciton diffusion length throughout the entire bulk of the active layer. This completely eliminates the loss caused by short exciton diffusion length because ideally, all excitons are dissociated before they decay [3]. This parameter is closely related to the charge separation efficiency, η_{CS}.

There were reports showing that device dissolved in the solvent chlorobenzene performed better than when dissolved in toluene [98]. The chlorobenzene-based device of the structure ITO/PEDOT/MDMO-PPV:PCBM/LiF/Al demonstrated a more efficient EQE and a higher FF, which were attributed to the higher charge carrier mobility. The J_{SC} of the device was 5.25 mA/cm^2 compared to 2.33 mA/cm^2 from the toluene-based device. As a result, the PCEs were also dramatically different, with 2.5% and 0.9% respectively (see Fig. 11). It was observed that in the chlorobenzene-cast film, the size of the PCBM clusters was less than 100 nm whereas in the toluene-cast film, the size of the PCBM clusters was in the order of micrometer. Also, chlorobenzene-cast film gave a more homogenous and bicontinuous blend while toluene-cast film gave a non-bicontinuous blend [9]. This was mainly attributed to the higher solubility of PCBM in chlorobenzene [99].

Influence of solvents on PCDTBT:PC$_{70}$BM blend was also reported [39]. The films were dissolved in chloroform (CF), chlorobenzene (CB) and dichlorobenzene (DCB) respectively. Large

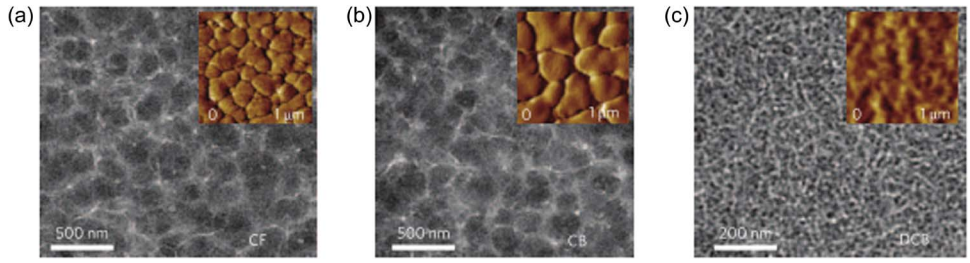

Fig. 12. TEM images of PCDTBT:$PC_{70}BM$ spin-cast from (a) CF, (b) CB, and (c) DCB. Inset shows the surface phase images measured by atomic force microscopy (AFM) [39].

dark clusters were observed in CF (200 nm) and CB films (300 nm) while clearly defined nanostructure phase separation was observed in DCB films, as shown in Fig. 12. The nanoscale phase separation was favorable as it led to an increased EQE. The formation of well-connected percolated networks also contributed to the enhanced J_{SC} and FF.

Around the same time as [39], Liang *et al.* [17] also reported a PCE of about 6%, using the novel semiconducting polymer PTB4 as donor and PCBM as acceptor. This low-bandgap ($\sim$1.6 eV) and good hole mobility polymer showed efficient absorption around the region with highest photon flux in the solar spectrum (about 700 nm), good solubility in organic solvent and suitable miscibility with fulleride acceptor. It also has a relatively low-lying HOMO with enhanced V_{OC}. However, due to the non-optimized morphology of the solar cell device, under AM1.5 (100 mW/cm^2), the J_{SC} and the FF of this OSC were significantly low and resulted in a modest PCE of 3.1%. This was attributed to the bulky side chains of PTB4 that reduced its miscibility with PCBM, resulting in lesser interfacial areas for charge separation. This morphological problem was addressed by using mixed solvents in preparing the polymer/fullerene spin-coating solution [100]. Dichlorobenzene/1,8-diiooctane (97/3, v/v) produced films with no large features as observed in the PTB4:PCBM blend film. The J_{SC}, V_{OC} and FF were all improved and it displayed a PCE of 5.9%. With spectral mismatch factor of 0.965 accounted for, the PCE of the PTB4: The PCBM device was about 6.1%, giving a 90% enhancement.

In the following year, after an extensive structural optimization, the same group synthesized another novel donor, poly[[4,8-bis[(2-ethylhexyl)oxy]benzo[1,2-b:4,5-b′] dithiophene-2,6-diyl][3-fluoro-2-[(2-ethylhexyl)carbonyl] thieno[3,4-b]thiophenediyl]] (PTB7) and they reported an even higher PCE device of 7.4%. This donor material exhibited excellent PV properties, with good solubility in organic solvents, high hole mobility of $5.8 \times 10 - 4\ \mathrm{cm^2V^{-1}}s^{-1}$ and strong absorption from 550 nm to 750 nm. However, the absorption was relatively weak from 300 nm to 500 nm. Hence, the acceptor $PC_{70}BM$ was used to compensate the relatively weak absorption region of PTB7. The resulting PTB7:$PC_{70}BM$ blend had a strong absorption from 300 nm to about 800 nm. With this combination, the device exhibited $J_{SC} = 13.56$ mA/cm^2, $V_{OC} = 0.75$ V, FF $= 0.59$, and PCE $= 6.02\%$, which was similar to the PTB4:PCBM blend results [17].

Though the result was satisfactory, mixed solvent of chlorobenzene/1,8-diiodoctane was attempted to enhance the performance of PTB7:$PC_{70}BM$ blend. The resulting device showed $J_{SC} = 14.5$ mA/cm^2, $V_{OC} = 0.74$ V, FF $= 0.69$ and PCE $= 7.4\%$, about 20% enhancement compared to the device without the use of mixed solvents. The morphology of the blend film was much more uniform and there was no large phase separation, showing the good miscibility between the PTB7 and the $PC_{70}BM$, and the smooth formation of interpenetrating networks. FF and J_{SC} were improved.

The concept of mixed solvent was also applied to conjugated polymer PBDTTPD blended with $PC_{70}BM$ [101]. By adding a mixture of two different additives, 1,8-diiodooctane (DIO) and 1-chloronaphthalene (CN), into the host solvent (ortho-dichlorobenzene (ODCB) or chlorobenzene (CB)), the performance of the PBDTTPD:$PC_{70}BM$ blend was improved. Different ratios of CN to DIO were tested to obtain the morphology of interpenetrating networks with optimized

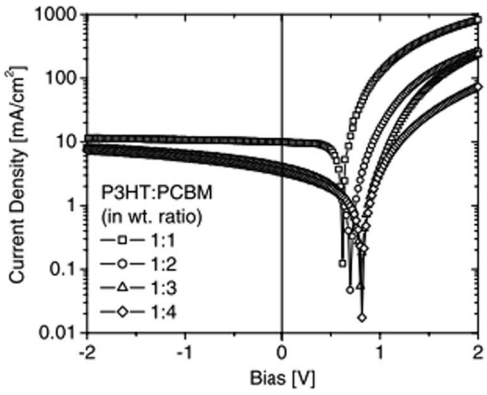

Fig. 13. J-V characteristics for photovoltaic devices with P3HT:PCBM active layer containing 1 : 1, 1 : 2, 1 : 3, and 1 : 4 wt/wt ratio [102].

domain sizes. With CN content of 10% (v/v) and DIO content of 1% (v/v), an optimized device with the following PV characteristics was successfully obtained: $V_{OC} = 0.87$ V, $J_{SC} = 11$ mA/cm^2, FF $= 0.67$ and PCE $= 6.4\%$, demonstrating an enhancement of 137%.

As for blend ratio, the formerly highest reported PCE for P3HT:PCBM device was 3.5% using 1 : 2 wt/wt ratio [24]. However, there were other reports on higher PCE using 1 : 1 wt/wt ratio. The absorption of P3HT was significantly shifted with an increasing amount of PCBM in the blend [102]. This spectra modification was attributed to the lowering of inter-chain interaction due to the presence of PCBM molecules and the non-photoinduced charge transfer between P3HT and PCBM in solid sate. As a result, the device with higher amount of PCBM exhibited sharp reduction in the J_{SC}. On the contrary, with increasing amount of PCBM, the V_{OC} value increased, as observed from Fig. 13. Best performance was observed from devices with 1 : 1 ratio, giving a PCE $= 3.85\%$. In addition to that, it is widely believed that the low hole mobility in donor polymer led to the low photocurrent [12], [103]. As such, for P3HT:PCBM with 1 : 1 wt/wt ratio, they tend to transport holes more efficiently compared to the device with 1 : 2 wt/wt ratio and this resulted in a more balanced electron and hole transport.

In the case of PCDTBT:PC_{70}BM, the higher the amount of PC_{70}BM, the clearer the nanoscale phase separation. At a ratio of 1 : 4, a fibrillar PCDTBT nanostructure was the most pronounced, meaning that the higher amount of PC_{70}BM led to a longer and better connected PCDTBT network [39]. Further investigation revealed that the morphology of PCDTBT:PC_{70}BM was laterally oriented as opposed to P3HT:PC_{70}BM which was vertically well-connected. Therefore, to have a high PCE BHJ cell, the ideal morphology of the cell should be "column-like".

Other than choice of solvents and blend ratio, thermal annealing also affects the PCE of a device. Most of the time, for a BHJ OSC, the FF is low due to the space-charge effects and the series resistance is high due to the disordered structure [104]. To have a high PCE device, the thickness of the device needs to be increased to absorb the solar radiation efficiently but this will further increase the series resistance as well. Li *et al.* [97] demonstrated that thermal annealing could significantly reduce the series resistance of the BHJ OSC. They controlled the growth rate of the active layer from solution to solid state and the FF increased to a value of more than 0.67. The high FF was believed to be due to the high thickness of the active layer, rending it free of pinholes and microcracks. After annealing for 10 minutes at 110 °C, the device showed $J_{SC} = 10.6$ mA/cm^2, $V_{OC} = 0.61$ V, FF $= 0.67$, and PCE $= 4.37\%$. Compared to the device without annealing, the PCE increased by 25%. Annealing smoothen the surface of the active layer and enable a defect-free contact with the metal cathode.

Padinger *et al.* [24] reported a postproduction treatment method involving annealing the device and simultaneously applying an external voltage. The device investigated was of the structure ITO/PEDOT/P3HT:PCBM/LiF/Al. Without annealing and without the external voltage,

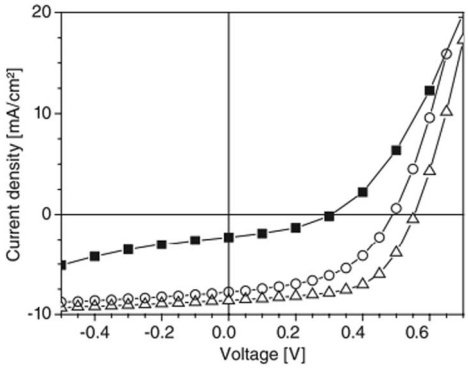

Fig. 14. Graph of current versus voltage of P3HT:PCBM solar cells under white light illumination with 800 W/m^2 irradiation intensity for as-produced solar cell (filled square), annealed solar cell (open circles), and cell simultaneously treated by annealing and applying an external electric field (open triangles) [24].

the device exhibited the following PV characteristics: $J_{SC} = 2.5$ mA/cm^2, $V_{OC} = 0.3$ V, FF $= 0.4$, and PCE $= 0.4\%$ under 800 W/m^2. The low PCE was attributed to the low mobility of charges inside the active layer. A study from Zhao *et al.* [25] illustrated that when P3HT was annealed to a temperature higher than its glass-transition temperature, an enhanced crystallization of the polymer took place. This helped to increase the hole conductivity of P3HT dramatically [26]. Thus, the device was subjected to annealing of 75 °C for 4 minutes. All the PV properties improved significantly: $J_{SC} = 7.5$ mA/cm^2, $V_{OC} = 0.5$ V, FF $= 0.57$, and PCE $= 2.5\%$. To further improve the device performance, during the annealing of the device, an external voltage greater than the VOC was applied simultaneously and this gave an even better results: $J_{SC} = 8.5$ mA/cm^2, $V_{OC} = 0.55$ V, FF $= 0.6$, and PCE $= 3.5\%$. The results were shown in Fig. 14. The improvements observed were presumed to be due to the additional injection of charges into the polymer bulk, which supported an orientation of the polymer chains inside the photoactive matrix in the direction of the electric field, when external voltage was applied simultaneously [24].

In year 2005, the performance of the OSC was further improved by Ma *et al.* [23] by addressing the thermal stability issue. There were concerns about instability of device at elevated temperatures and this hindered large-scale implementation. By applying specific device-fabrication conditions and postproduction annealing at 150 °C, the device of structure ITO/PEDOT/P3HT:PCBM/Al reported a PCE of 5% under AM1.5 (80 mW/cm^2). Before employing heat treatment, the solar cell exhibited a poor performance with $J_{SC} = 3.83$ mA/cm^2, $V_{OC} = 0.6$ V, FF $= 0.3$, and PCE $= 0.82\%$. After annealing at 150 °C for 30 minutes, the performance of the device improved to $J_{SC} = 9.5$ mA/cm^2, $V_{OC} = 0.63$ V, FF $= 0.68$, and PCE $= 5.0\%$. There were attempts [24], [105] to anneal the OSC at higher temperature but they were halted by the steep decrease in PCE after annealing for only a few seconds at 130 °C or a few minutes at 75 °C. Hoppe *et al.* [99] later revealed that this was due to the formation of large PCBM aggregates that degraded the morphology of the film. To overcome this, chlorobenzene was used as the solvent, and the P3HT:PCBM ratio and concentration were reduced [23]. The resulting device displayed exceptional efficiency and outstanding thermal stability even after subjected to heat for hours at such a high temperature. This excellent performance was due to the formation of thermally stable nanoscale, interpenetrating donor-acceptor network and stable phase separation for efficient charge separation and transport. There were a few other groups who investigated the thermal annealing effect on the polymer P3HT:PCBM blend as well, and the PCE reported were around 5% [23], [27].

Thermal annealing and controlled solvent evaporation that had been proven to be crucial for optimizing the charge separation and the charge transport within the BHJ structure were not

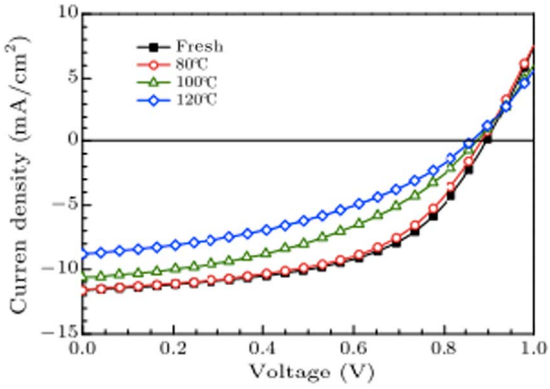

Fig. 15. J-V Characteristics of the PCDTBT:$PC_{70}BM$ device under thermal annealing at different temperatures [4].

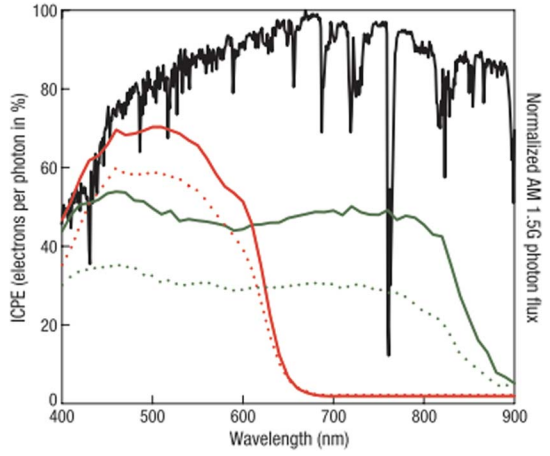

Fig. 16. IPCE spectra of P3HT:PCBM before (dotted red line) and after (solid red line) annealing and PCPDBT:$PC_{70}BM$ with (solid green line) and without (dotted green line) the use of octanedithiol [15]. The AM1.5G reference spectrum (black line) is shown for reference [107].

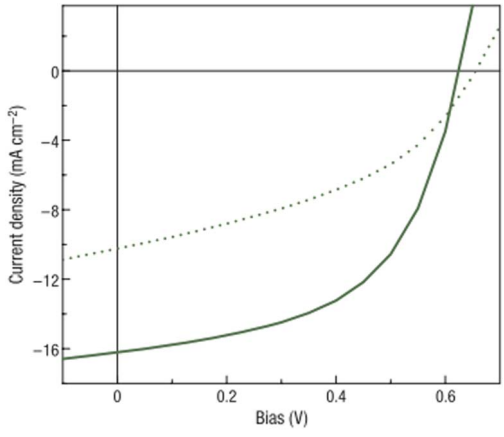

Fig. 17. Current-voltage characteristics of the PCPDBT:$PC_{70}BM$ devices used for the IPCE measurement, processed with (solid line) and without (dotted line) octanedithiol under AM1.5 (100 mW/cm^2) [15].

TABLE 3

Summary of device PCEs and the optimized parameters

Year	Device Structure	J_{sc} (mA /cm^2)	V_{oc} (V)	FF	PCE (%)	Optimization	Ref
2001	ITO/PEDOT/MDMO-PPV:PCBM/LiF/Al	5.25	0.82	0.610	2.5	Morphological Control	[99]
2003	ITO/PEDOT/P3HT:PCBM/LiF/Al	8.5	0.55	0.600	3.5	Morphological Control	[24]
2004	ITO/PEDOT:PSS/PFO-DBT:PCBM/Ba/Al	5.18	0.95	0.460	2.24	Material Engineering	[22]
2005	ITO/PEDOT/P3HT:PCBM/Al	10.6	0.61	0.674	4.37	Morphological Control	[97]
2005	ITO/PEDOT/P3HT:PCBM/Al	9.5	0.63	0.680	5.0	Morphological Control	[23]
2006	ITO/PEDOT:PSS/P3HT:PCBM/TiO_X/Al	11.1	0.61	0.660	5.0	Material Engineering	[13]
2006	ITO/PEDOT:PSS/P3HT:PCBM/Ca	8.95	0.59	0.596	3.18	Material Engineering	[65]
2006	ITO/V_2O_5/P3HT:PCBM/Ca	8.83	0.59	0.591	3.10	Material Engineering	[65]
2006	ITO/MoO_3/P3HT:PCBM/Ca	8.94	0.60	0.619	3.33	Material Engineering	[65]
2006	ITO/PEDOT/PCPDTBT:$PC_{70}BM$/Al	11.0	0.65	0.470	3.2	Material Engineering	[47]
2007	ITO/PEDOT:PSS/PCDTBT:PCBM/Al	6.92	0.89	0.630	3.6	Material Engineering	[35]
2007	ITO/PEDOT:PSS/PCPDTBT:$PC_{70}BM$/Al	16.2	0.62	0.550	5.5	Morphological Control	[15]
2007	ITO/NiO/P3HT:PCBM/LiF/Al	11.3	0.64	0.693	5.16	Material Engineering	[64]
2007	ITO/PEDOT:PSS/APFO-15:PCBM/LiF/Al	6.0	1	0.630	3.7	Material Engineering, Morphological Control	[36]
2009	ITO/PEDOT:PSS/PCDTBT:$PC_{70}BM$/Al	10.6	0.88	0.660	6.1	Morphological Control, Interfacial Layer Insertion	[39]
2009	ITO/PEDOT:PSS/PTB4:PCBM/Ca/Al	13.0	0.74	0.614	6.1	Morphological Control	[17]
2009	ITO/PEDOT:PSS/PCDTBT:PCBM/LiF/Al	9.5	0.91	0.600	5.2	Layer Thickness Optimization	[40]
2009	ITO/PEDOT:PSS/PBDTTT-E:$PC_{70}BM$/Ca/Al	13.2	0.62	0.630	5.15	Material Engineering	[43]
2009	ITO/PEDOT:PSS/PBDTTT-C:$PC_{70}BM$/Ca/Al	14.7	0.7	0.641	6.58	Material Engineering	[44]
2009	ITO/PEDOT:PSS/PBDT	15.2	0.76	0.669	7.73	Material	[43]
	TT-CF:$PC_{70}BM$/Ca/Al					Engineering	
2010	ITO/PEDOT:PSS/PTB7:$PC_{70}BM$/Ca/Al	14.5	0.74	0.690	7.4	Morphological Control	[11]
2010	ITO/PEDOT:PSS/PBDTTPD:$PC_{70}BM$/LiF/Al	9.81	0.85	0.660	5.5	Material Engineering	[60]
2011	ITO/PEDOT:PSS/PCDTBT:$PC_{70}BM$/LiF/Al	11.6	0.90	0.537	5.6	Material Engineering	[4]
2011	ITO/MoO_3/PCDTBT:$PC_{70}BM$/TiO_X/Al	10.88	0.89	0.670	6.5	Interfacial Layer Insertion, Layer Thickness Optimization	[38]

TABLE 3 *(continued)*

2011	ITO/PEDOT:PSS/PBDTTT-E:$PC_{70}BM$/Ca/Al	11.53	0.66	0.547	4.16	Material Engineering	[59]
2011	ITO/PEDOT:PSS/PBDTTT-E-T:$PC_{70}BM$/Ca/Al	14.59	0.68	0.626	6.21	Material Engineering	[59]
2011	ITO/PEDOT:PSS/PBDTTT-C:$PC_{70}BM$/Ca/Al	15.51	0.70	0.592	6.43	Material Engineering	[59]
2011	ITO/PEDOT:PSS/PBDTTT-C-T:$PC_{70}BM$/Ca/Al	17.48	0.74	0.587	7.59	Material Engineering	[59]
2011	ITO/PEDOT:PSS/PBDTTT-S:$PC_{70}BM$/Ca/Al	14.1	0.76	0.58	6.22	Material Engineering	[45]
2012	ITO/PEDOT:PSS/PCDTBT:PCBM/ TiO_X/Al	11.32	0.88	0.690	6.9	Layer Thickness Optimization	[41]
2012	ITO/PEDOT:PSS/PBDTTPD:PCBM/BCP/Al	10.89	0.93	0.700	7.1	Morphological Control	[102]
2012	ITO/PEDOT:PSS/PBDTTPD:$PC_{70}BM$/BCP/Al	11.0	0.87	0.67	6.4	Morphological Control	[102]

successful for PCPDTBT:$PC_{70}BM$ solar cells [15]. Annealing the device, even at a relatively low temperature of 80–120 °C, reduced the FF, J_{SC}, and V_{OC}, as shown in Fig. 15 [4]. Thus, in order to promote the performance of these devices, the temperature used to remove the casting solvent should not be more than 80 °C. The decreased performance was attributed to the over-sized phase separation. The nanoscale phase separation in BHJ materials must be less than 20 nm because the exciton diffusion length is about or less than 10 nm. The over-sized phase separation induces increased in surface roughness and exciton trap density in the active layer, which in turn leads to trap-assisted interfacial recombination. This reduced the charge extraction efficiency at the interfaces and resulted in some loss in the overall performance. Exposure to elevated temperatures in air led to accelerated oxidation of the polymer backbone, destroying the materials' properties.

Nonetheless, in another report [106], PCDTBT demonstrated outstanding ability to withstand exposure to high temperatures. Based on the results of field-effect transistors (FET) devices, the transport mobility increased steadily after exposure to elevated temperatures of up to 170 °C to and they remained stable even up to 350 °C. Comparatively, devices based on P3HT reported degradation after exposure to 200 °C. However, the remarkable thermal stability was observed only for highest-molecular-weight materials.

Later, Peet *et al.* [15] published a report on the successful morphological control of BHJ devices where thermal annealing was either undesirable or ineffective. By incorporating a small concentration of alkanethiols in the active PCPDTBT:$PC_{70}BM$ BHJ layer, the film absorption peak red-shifted by 41 nm to 800 nm. The PCPDTBT chains interacted more strongly with improved local structural order compared to the films processed from pure chlorobenzene. There was also an increase in the number of collected charge carriers and an increase in carrier lifetime. The group compared the devices processed from chlorobenzene and from chlorobenzene with 24 mg/ml volume alkanedithiols with different chain lengths. The most significant improvement in terms of J_{SC} and FF was observed in the device casted from the chlorobenzene containing octanedithiol. The IPCE spectra of the PCPDTBT:$PC_{70}BM$ devices (with and without the use of octanedithiol) and the P3HT:PCBM devices (before and after thermal annealing) are shown in Fig. 16.

From Fig. 17, it was observed that the photon absorption by the PCPDTBT:$PC_{70}BM$ devices covered a much broader range as compared to P3HT:PCBM devices. With the addition of octanedithiol, the IPCE increased by about 60%. The most repeatable series of high-efficiency device had $J_{SC} = 16.2$ mA/cm^2, $V_{OC} = 0.62$ V, FF $= 0.55$ and PCE $= 5.5\%$ under 100 mW/cm^2 as shown in Fig. 17. The improvement in the J_{SC} and FF were apparent with the addition of octanedithiol.

3. Outlook

From Table 2, we can see the performance of BHJ PSCs rises from a PCE of 2.5% to 7.73% in a mere decade time. Problems such as mismatch of materials absorption with the solar spectrum, less favorable energy levels between donor and acceptor, and non-optimized morphology of the blend are tackled progressively as scientists and researchers gain more understanding in the field of OSCs. As compared to the matured field of inorganic solar cells, OSCs are considered relatively new and hence, there are still many ideas yet to be explored and developed.

Among the examples presented in the article, there are a few donor materials that show promising performance and based on their characteristics, we believe that they can be further enhanced. They are APFO-15, PBDTTPD, and PCDTBT. These polymers have a low-lying HOMO and thus, a high V_{OC} exceeding 0.8 V [4], [35], [36], [39]–[41], [60], [101]. However, their J_{SC} values are relatively low compared to other low-bandgap polymers that achieve a J_{SC} of more than 13 mA/cm^2 [11], [17], [43]–[45], [59]. APFO-15 has a relatively lower J_{SC} because of its weak absorption in the region around 300 nm to 350 nm [108]. For PBDTTPD, it has limited solubility in the solvent ODCB. Although this limitation is overcome by the use of two processing additives, CN and DIO, the maximum J_{SC} value achieved is only around 11 mA/cm^2. As for PCDTBT, this polymer has lateral morphology, as opposed to the ideal 'column-like' morphology for efficient charge transfer to the electrodes. It exhibits increased interface recombination and lower η_{CC} because of the corresponding increase in the path length [41].

Since V_{OC} value is largely controlled by the difference between the HOMO of the donor and the LUMO of the acceptor, its enhancement is mostly restricted to material engineering. Whereas for J_{SC}, it can be enhanced through numerous approaches, such as improving the absorption of the active layer, increasing the η_{CS}, η_{CC}, lower the rate of recombination and enhancing the carrier mobilities. Therefore, future investigations on improving the performance of BHJ PSC should focus on the enhancement of J_{SC} especially on the materials with low-lying HOMO. Nonetheless, among the polymers, PCDTBT appears to be the most promising. Other than its high PCE performance, PCDTBT-based devices also demonstrate a lifetime of approaching 7 years, which is impressively higher than P3HT-based devices (about 3 years) [109]. The future of this polymer seemed bright if the J_{SC} could be further improved.

Of all the optimization approaches discussed in the article, it is shown that morphology plays a crucial role in determining the performance of the solar cells. When the morphology of an OSC is optimized, the PCE enhancement is significant with increment of at least 20% [11] up to 775% [24], and the increment is largely due to the increment in J_{SC}. Nonetheless, the control over the morphology of material is challenging as it could be affected by sensitive parameters such as solvent choice, blend ratio, and thermal annealing.

In recent years, there are reports on successful increment in J_{SC} via the incorporation of advanced structure such as metal nanostructures into the OSC [110]–[115]. These metal nanostructures induce plasmonic effects in the device upon light incident, leading to increased light absorption and eventually higher J_{SC} values. A few known plasmonic mechanisms are light scattering, propagating waveguide modes based on photonic waveguide or surface plasmon polariton (SPP), and high near-field intensities due to localized surface plasmon resonance (LSPR). For scattering mechanism, the positions of the metal nanostructures are very important as they affect the scattering direction [116]. If the light is scattered beyond the critical angle for reflection, it remains trapped in the cell thus increasing the optical path length for better absorption. As for the propagating waveguide modes, it enhances light absorption by redirecting the light horizontally and the power in the propagating waveguide is partially absorbed in the semiconductor layer, exciting electron-hole pairs along the way. On the other hand, depending on the size and shape of the metallic particle, LSPR results in strong near-field enhancement. Strong field contributes to an increase in absorption [117].

Some OSC structures made use of more than one plasmonic mechanisms [118]. An OSC made up of semi-transparent silver (Ag) nanowire anode and a continuous Ag cathode demonstrated enhancement in PCE [118]. Under Transverse Magnetic (TM) and Transverse Electric

(TE) polarized illuminations, the cell showed absorption enhancement induced by SPR effect and waveguide modes respectively. The EQE of the cell was considerably high. Other than nanowire, OSC that employed nanohole arrays as electrode also supported short-range SPP mode, which brought about broadband absorption enhancement [119]. On top of that, a hybrid structure, combining the metallic nanodisc and nanohole arrays, permitted the coupling of localized SPP modes with the single-interface SPP modes. These lead to even greater absorption enhancement [120]. Although most of these cells have yet to reach the 10% efficiency, these types of plasmonic cells are appealing as they are able to increase light absorption without increasing the cell thickness.

There are a few other types of OSCs that have already achieved PCEs of more than 10%. One of them is the perovskite-based OSC that shows very promising results with a PCE of about 16%. The significant progress made by this type of OSC attracts much attention. However, since the organo-lead halides polymer used in this cell was expensive and complex, Christians *et al.* [121] tried to replace it with copper iodide, an inorganic hole conducting material. The cell gave a PCE of only about 6% due to high recombination. Nonetheless, the cell exhibited excellent electrical conductivity. It was believed that if the recombination could be reduced, this cell could be a cost-effective competitor to spiro-OMeTAD.

Another type of cell, namely Heliatek cell, also reported a high PCE of about 12% [122]. It is based on small-molecules. Two different absorber materials were used for stronger photon absorption. One drawback of this cell is that the production costs are relatively high [123]. Since most of the OSCs that achieved PCE of more than 10% are also associated with high material costs and/or high production costs, it is hoped that a low-cost but high PCE OSC could be realized soon. In addition to that, the lifetime of OSC is also equally important. As mentioned, an estimated PCE of 5% to 10% and a lifetime of 5 to 10 years are required for an OSC to be considered as cost-efficient. Therefore, to be viable for commercialization as well, an OSC needs to be low-cost, have high PCE and long lifetime.

4. Conclusion

A comprehensive review and detailed discussion on the optimization development of BHJ OSC have been carried out. Optimization through material engineering are done by utilizing less electron-rich groups in the polymer, modifying its side groups, designing low-bandgap polymers, choosing an acceptor with absorption at complementary region and structural fine-tuning to improve the V_{OC} and J_{SC}. Efficient charge collection at the electrodes is ensured by choosing buffer layers with appropriate energy levels relative to the active layer materials and electrodes. The electron-blocking layer prevents electron leakage and facilitates hole extraction at the anode. Hole-blocking layer prevents holes in the donor phase to flow into cathode, facilitates electron extraction at the cathode and/or redistributes the light intensity within the BHJ blend. Layer thickness optimization is also proven to be crucial to ensure high absorption of the device and it is dependent on the materials' absorption coefficient, recombination, charge carrier mobility and cost. Last but not least, careful morphological control especially in terms of choice of solvents, blend ratio of donor to acceptor and thermal annealing conditions lead to the significant performance improvement of OSCs. The optimization efforts in these areas demonstrated a positive future for OSCs. Together with the successful incorporation of advanced structure into the organic devices and positive development in long operating lifetime, it is anticipated that OSC will be able to compete with its inorganic counterpart to be a true low-cost and high PCE solar technology, with long operating lifetime.

References

[1] J. He *et al.*, "Plasmonic nanostructure for enhanced light absorption in ultrathin silicon solar cells," *Adv. Optoelectron.*, vol. 5, pp. 1–8, 2012.

[2] K. D. G. I. Jayawardena *et al.*, "'Inorganics-inorganics': Recent developments and outlook for 4G polymer solar cells," *Nanoscale*, vol. 5, no. 18, pp. 8411–8427, 2013.

[3] H. Hoppe and N. S. Sariciftci, "Organic solar cells: An overview," *J. Mater. Res.*, vol. 19, no. 7, pp. 1924–1945, Jul. 2004.
[4] S.-P. Yang *et al.*, "Highly efficient PCDTBT:PC71BM based photovoltaic devices without thermal annealing treatment," *Chin. Phys. Lett.*, vol. 28, no. 12, pp. 128401-1–128401-4, Dec. 2011.
[5] J. J. M. Halls, K. Pichler, R. H. Friend, S. C. Moratti, and A. B. Holmes, "Exciton diffusion and dissociation in a poly(p-phenylenevinylene)/C_{60} heterojunction photovoltaic cell," *Appl. Phys. Lett.*, vol. 68, no. 22, pp. 3120–3122, May 1996.
[6] C. D. Dimitrakopoulos and D. J. Mascaro, "Organic thin-film transistors: A review of recent advances," *IBM J. Res. Develop.*, vol. 45, no. 1, pp. 11–27, Jan. 2001.
[7] G. Dennler, M. C. Scharber, and C. J. Brabec, "Polymer-fullerene bulk-heterojunction solar cells," *Adv. Mater.*, vol. 21, no. 13, pp. 1323–1338, 2009.
[8] J. C. Hummelen *et al.*, "Preparation and characterization of fulleroid and methanofullerene derivatives," *J. Org. Chem.*, vol. 60, no. 3, pp. 532–538, 1995.
[9] B. C. Thompson and J. M. J. Fréchet, "Polymer-fullerene composite solar cells," *Angewandte Chemie Int. Ed. Engl.*, vol. 47, no. 1, pp. 58–77, Dec. 2008.
[10] F. Yang, M. Shtein, and S. R. Forrest, "Controlled growth of a molecular bulk heterojunction photovoltaic cell," *Nat. Mater.*, vol. 4, pp. 37–41, 2005.
[11] Y. Liang *et al.*, "For the bright future-bulk heterojunction polymer solar cells with power conversion efficiency of 7.4%.," *Adv. Mater.*, vol. 22, no. 20, pp. E135–E138, 2010.
[12] C. J. Brabec, "Organic photovoltaics: Technology and market," *Solar Energy Mater. Solar Cells*, vol. 83, no. 2–3, pp. 273–292, Jun. 2004.
[13] G. Yu, J. Gao, J. C. Hummelen, F. Wudl, and A. J. Heeger, "Polymer photovoltaic cells: Enhanced efficiencies via a network of internal donor-acceptor heterojunctions," *Science*, vol. 270, no. 5243, pp. 1789–1791, Dec. 1995.
[14] J. Y. Kim *et al.*, "New architecture for high-efficiency polymer photovoltaic cells using solution-based titanium oxide as an optical spacer," *Adv. Mater.*, vol. 18, no. 5, pp. 572–576, Mar. 2006.
[15] J. Peet *et al.*, "Efficiency enhancement in low-bandgap polymer solar cells by processing with alkane dithiols," *Nat. Mater.*, vol. 6, no. 7, pp. 497–500, 2007.
[16] J. Y. Kim *et al.*, "Efficient tandem polymer solar cells fabricated by all-solution processing," *Science*, vol. 317, pp. 222–225, 2007.
[17] Y. Liang *et al.*, "Highly efficient solar cell polymers developed via fine-tuning of structural and electronic properties," *J. Am. Chem. Soc.*, vol. 131, no. 22, pp. 7792–7799, 2009.
[18] M. A. Green, K. Emery, Y. Hishikawa, and W. Warta, "Solar cell efficiency tables (version 37)," *Progr. Photovoltaics Res. Appl.*, vol. 19, no. 1, pp. 84–92, Jan. 2011.
[19] R. F. Service, "Outlook brightens for plastic solar cells," *Science*, vol. 332, pp. 293, Apr. 2011.
[20] J. D. Servaites, M. A. Ratner, and T. J. Marks, "Organic solar cells: A new look at traditional models," *Energy Environ. Sci.*, vol. 4, no. 11, pp. 4410–4422, 2011.
[21] G. Li, R. Zhu, and Y. Yang, "Polymer solar cells," *Nat. Photon.*, vol. 6, no. 3, pp. 153–161, 2012.
[22] Q. M. Zhou *et al.*, "Fluorene-based low band-gap copolymers for high performance photovoltaic devices," *Appl. Phys. Lett.*, vol. 84, no. 10, pp. 1635–1655, Mar. 2004.
[23] W. Ma, C. Yang, X. Gong, K. Lee, and A. J. Heeger, "Thermally stable, efficient polymer solar cells with nanoscale control of the interpenetrating network morphology," *Adv. Functional Mater.*, vol. 15, no. 10, pp. 1617–1622, Oct. 2005.
[24] F. Padinger, R. S. Rittberger, and N. S. Sariciftci, "Effects of postproduction treatment on plastic solar cells," *Adv. Functional Mater.*, vol. 13, no. 1, pp. 85–88, Jan. 2003.
[25] Y. Zhao, G. Yuan, P. Roche, and M. Leclerc, "A calorimetric study of the phase transitions in poly(3-hexylthiophene)," *Polymer*, vol. 36, no. 11, pp. 2211–2214, 1995.
[26] K. Beih *et al.*, "Electron trapping in dye/polymer blend photovoltaic cells," *Adv. Mater.*, vol. 12, no. 17, pp. 1270–1274, 2000.
[27] M. Reyes-Reyes, K. Kim, and D. L. Carroll, "High efficiency photovoltaic devices based on annealed poly (3-hexylthiophene) and 1-(3-methoxycarbonyl)-propyl-1- phenyl-(6,6)C_{61} blends," *Appl. Phys. Lett.*, vol. 87, no. 8, pp. 083506-1–083506-3, Aug. 2005.
[28] P. Schilinsky, C. Waldauf, and C. J. Brabec, "Recombination and loss analysis in polythiophene based bulk heterojunction photodetectors," *Appl. Phys. Lett.*, vol. 81, no. 20, pp. 3885–3887, Nov. 2002.
[29] H. Sirringhaus *et al.*, "Two-dimensional charge transport in self-organized, high-mobility conjugated polymers," *Nature*, vol. 401, pp. 685–688, 1999.
[30] J.-J. Yun *et al.*, "Chlorophyll-layer-inserted poly(3-hexyl-thiophene) solar cell having a high light-to-current conversion efficiency up to 1.48%," *Appl. Phys. Lett.*, vol. 87, no. 12, pp. 123102, Sep. 2005.
[31] C. W. Tang, "Multilayer organic photovoltaic elements," U.S. Patent 4 164 431, Aug. 14 1979.
[32] C. J. Brabec *et al.*, "The influence of materials work function on the open circuit voltage of plastic solar cells," *Thin Solid Films*, vol. 403/404, pp. 368–372, 2002.
[33] H. Kim, S. H. Jin, H. Suh, and K. Lee, "Origin of the open circuit voltage in conjugated polymer-fullerene photovoltaic cells," *Proc. Org. Photovoltaics IV*, 2004, vol. 5215, pp. 111–118.
[34] M. C. Scharber *et al.*, "Design rules for donors in bulk-heterojunction solar cells—Towards 10% energy-conversion efficiency," *Adv. Mater.*, vol. 18, no. 6, pp. 789–794, Mar. 2006.
[35] N. Blouin, A. Michaud, and M. Leclerc, "A low-bandgap poly(2,7-carbazole) derivative for use in high-performance solar cells," *Adv. Mater.*, vol. 19, no. 17, pp. 2295–2300, Sep. 2007.
[36] A. Gadisa *et al.*, "A new donor-acceptor-donor polyfluorene copolymer with balanced electron and hole mobility," *Adv. Functional Mater.*, vol. 17, no. 18, pp. 3836–3842, Dec. 2007.
[37] L. J. Huo, J. H. Hou, S. Q. Zhang, H. Y. Chen, and Y. Yang, "A polybenzo[1,2- b:4,5-b']dithiophene derivative with deep HOMO level and its application in high-performance polymer solar cells," *Angewandte Chemie Int. Ed.*, vol. 49, no. 8, pp. 1500–1503, Feb. 2010.

[38] Y. Sun *et al.*, "Efficient, air-stable bulk heterojunction polymer solar cells using MoO(x) as the anode interfacial layer," *Adv. Mater.*, vol. 23, no. 19, pp. 2226–2230, May 2011.
[39] S. Cho *et al.*, "Bulk heterojunction solar cells with internal quantum efficiency approaching 100%," *Nat. Photon.*, vol. 3, pp. 297–303, 2009.
[40] T.-Y. Chu *et al.*, "Highly efficient polycarbazole-based organic photovoltaic devices," *Appl. Phys. Lett.*, vol. 95, no. 6, pp. 063304-1–063304-3, Aug. 2009.
[41] J. S. Moon, J. Jo, and A. J. Heeger, "Nanomorphology of PCDTBT:PC70BM bulk heterojunction solar cells," *Adv. Energy Mater.*, vol. 2, no. 3, pp. 304–308, Mar. 2012.
[42] J. Hou and X. Guo, "Active layer materials for organic solar cells," *Organic Solar Cells*, W. C. H. Choy, Ed. London, U.K.: Springer-Verlag, 2013, pp. 17–42.
[43] H. Chen *et al.*, "Polymer solar cells with enhanced open-circuit voltage and efficiency," *Nat. Photon.*, vol. 3, pp. 649–653, Nov. 2009.
[44] J. Hou *et al.*, "Synthesis of a low band gap polymer and its application in highly efficient polymer solar cells," *J. Amer. Chem. Soc.*, vol. 131, no. 43, pp. 15 586–15 587, 2009.
[45] Y. Huang *et al.*, "Sulfonyl: A new application of electron-withdrawing substituent in highly efficient photovoltaic polymer," *Chem. Commun.*, vol. 47, no. 31, pp. 8904–8906, 2011.
[46] *Reference Solar Spectral Irradiance: Air Mass 1.5*, Amer. Soc. Testing Mater. (ASTM) Std. G1592003. Available: http://rredc.nrel.gov/solar/spectra/am1.5/
[47] D. Mühlbacher, "High photovoltaic performance of a low-bandgap polymer," *Adv. Mater.*, vol. 18, no. 21, pp. 2884–2889, Nov. 2006.
[48] Y. J. Cheng, S. H. Yang, and C. S. Hsu, "Synthesis of conjugated polymers for organic solar cell applications," *Chem. Rev.*, vol. 109, no. 11, pp. 5868–5923, 2009.
[49] E. E. Havinga, W. Tenhoeve, and H. Wynberg, "Alternate donor-acceptor small-band-gap semiconducting polymers—Polysquaraines polycroconaines," *Synthetic. Metals*, vol. 55, no. 1, pp. 299–306, Mar.1993.
[50] Q. T. Zhang and J. M. Tour, "Low optical bandgap polythiophenes by an alternating donor/acceptor repeat unit strategy," *J. Amer. Chem. Soc.*, vol. 119, no. 21, pp. 5065–5066, 1997.
[51] A. Dhanabalan, J. K. J. Van Duren, P. A. Van Hal, J. L. J. Van Dongen, and R. A. J. Janssen, "Synthesis and characterization of a low bandgap conjugated polymer for bulk heterojunction photovoltaic cells," *Adv. Functional Mater.*, vol. 11, no. 4, pp. 255–262, Aug. 2001.
[52] J. K. J. Van Duren, A. Dhanabalan, P. A. Van Hal, and R. A. J. Janssen, "Low-bandgap polymer photovoltaic cells," *Synthetic Metals*, vol.121, no.1–3, pp.1587–1588, 2001.
[53] B. C. J. Brabec *et al.*, "A low-bandgap semiconducting polymer for photovoltaic devices and infrared emitting diodes," *Adv. Functional Mater.*, vol. 12, no. 10, pp. 709–712, 2002.
[54] C. Winder *et al.*, "Sensitization of low bandgap polymer bulk heterojunction solar cells," *Thin Solid Films*, vol. 403, pp. 373–379, 2002.
[55] M. Svensson *et al.*, "High-performance polymer solar cells of an alternating polyfluorene copolymer and a fullerene derivative," *Adv. Mater.*, vol. 15, no. 12, pp. 988–991, Jun.2003.
[56] K. G. Jespersen *et al.*, "The electronic states of polyfluorene copolymers with alternating donor-acceptor units," *J. Chem. Phys.*, vol. 121, no. 24, pp. 12613, Dec. 2004.
[57] A. M. Ballantyne *et al.*, "Studies of highly regioregular poly(3-hexylselenophene) for photovoltaic applications," *Adv. Mater.*, vol. 19, no. 24, pp. 4544–4547, 2007.
[58] X. Wang *et al.*, "Enhanced photocurrent spectral response in low-bandgap polyfluorene and C_{70}-derivative-based solar cells," *Adv. Functional Mater.*, vol. 15, no. 10, pp. 1665–1670, 2005.
[59] L. Huo *et al.*, "Replacing alkoxy groups with alkylthienyl groups: A feasible approach to improve the properties of photovoltaic polymers," *Angew. Chem. Int. Ed. Engl.*, vol. 50, no. 41, pp. 9697–702, Oct. 2011.
[60] Y. Zou *et al.*, "A thieno[3,4-c]pyrrole-4,6-dione-based copolymer for efficient solar cells," *J. Amer. Chem. Soc.*, vol. 132, no. 15, pp. 5330–5331, 2010.
[61] M. L. Zhang, H. Wang, and C. W. Tang, "Effect of the highest occupied molecular orbital energy level offset on organic heterojunction photovoltaic cells," *Appl. Phys. Lett.*, vol. 97, no. 14, pp. 143503-1–143503-3, Oct. 2010.
[62] L. J. A. Koster, V. D. Mihailetchi, and P. W. M. Blom, "Ultimate efficiency of polymer/fullerene bulk heterojunction solar cells," *Appl. Phys. Lett.*, vol. 88, no. 9, pp. 093511-1–093511-3, Feb. 2006.
[63] A. W. Hains and T. J. Marks, "High-efficiency hole extraction/electron-blocking layer to replace poly(3,4-ethylenedioxythiophene):poly(styrene sulfonate) in bulk-heterojunction polymer solar cells," *Appl. Phys. Lett.*, vol. 92, no. 2, pp. 023504–023506, Jan. 2008.
[64] M. D. Irwin, D. B. Buchholz, A. W. Hains, R. P. H. Chang, and T. J. Marks, "p-Type semiconducting nickel oxide as an efficiency-enhancing anode interfacial layer in polymer bulk-heterojunction solar cells," *Proc. Nat. Academy Sci.*, vol. 105, no. 8, pp. 2–6, 2007.
[65] V. Shrotriya, G. Li, Y. Yao, C.-W. Chu, and Y. Yang, "Transition metal oxides as the buffer layer for polymer photovoltaic cells," *Appl. Phys. Lett.*, vol. 88, no. 7, pp. 073508-1–073508-3, 2006.
[66] S. Khodabakhsh, B. M. Sanderson, J. Nelson, and T. S. Jones, "Using self-assembling dipole molecules to improve charge collection in molecular solar cells," *Adv. Functional Mater.*, vol. 16, no. 1, pp. 95–100, 2006.
[67] J. Hwang, F. Amy, and A. Kahn, "Spectroscopic study on sputtered PEDOT·PSS: Role of surface PSS layer," *Org. Electron.*, vol. 7, no. 5, pp. 387–396, 2006.
[68] A. C. Arias, M. Granstorm, D. S. Thomas, K. Petritsch, and R. H. Friend, "Doped conducting polymer-semiconducting polymer interfaces: Their use in organic photovoltaic devices," *Phys. Rev. B*, vol. 60, pp. 1854, 1999.
[69] S. Günes, H. Neugebauer, and N. S. Sariciftci, "Conjugated polymer-based organic solar cells.," *Chem. Rev.*, vol. 107, no. 4, pp. 1324–1338, Apr. 2007.
[70] P. Peumans and S. R. Forrest, "Very-high-efficiency double-heterostructure copper phthalocyanine/C_{60} photovoltaic cells," *Appl. Phys. Lett.*, vol. 79, pp. 126–128, 2001.

[71] H. Park, S. Chang, M. Smith, S. Gradečak, and J. Kong, "Interface engineering of graphene for universal applications as both anode and cathode in organic photovoltaics," *Sci. Rep.*, vol. 3, no. 1581, pp. 1–8, 2013.
[72] E. Voroshazi *et al.*, "Influence of cathode oxidation via the hole extraction layer in polymer:fullerene solar cells," *Org. Electron.*, vol. 12, no. 5, pp. 736–744, May 2011.
[73] H. Yan *et al.*, "High-performance hole-transport layers for polymer light-emitting diodes. Implementation of organosiloxane cross-linking chemistry in polymeric electroluminescent devices," *J. Amer. Chem. Soc.*, vol. 127, no. 9, pp. 3172–3183, 2005.
[74] M. P. De Jong, L. J. Van Ijzendoom, M. J. De Voight, "Stability of the interface between indium-tin-oxide and poly (3,4-ethylenedioxythiophene)/poly(styrenesulfonate) in polymer light-emitting diodes," *Appl. Phys. Lett.*, vol. 77, no. 14, pp. 2255, Oct. 2000.
[75] K. W. Wong *et al.*, "Blocking reactions between indium-tin oxide and poly(3,4-ethylene dioxythiophene):poly(styrene sulphonate) with a self-assembly monolayer," *Appl. Phys. Lett.*, vol. 80, no. 15, pp. 2788, Apr. 2002.
[76] J. Ni *et al.*, "MOCVD-derived highly transparent, conductive zinc- and tin-doped indium oxide thin films: Precursor synthesis, metastable phase film growth and characterization, and application as anodes in polymer light-emitting diodes," *J. Amer. Chem. Soc.*, vol. 127, no. 15, pp. 5613–5624, 2005.
[77] W. S. Koh, M. Pant, Y. A. Akimov, W. P. Goh, and Y. Li, "Three-dimensional optoelectronic model for organic bulk heterojunction solar cells," *IEEE J. Photovoltaics*, vol. 1, no. 1, pp. 84–92, Apr. 2011.
[78] D. C. Watters *et al.*, "Optimising the efficiency of carbazole co-polymer solar-cells by control over the metal cathode electrode," *Org. Electron.*, vol. 13, no. 8, pp. 1401–1408, 2012.
[79] A. W. Hains, A. B. F. Martinson, M. D. Irwin, H. Yan, and T. J. Marks, "Bulk-heterojunction organic solar cells: Interfacial engineering routes to increased open-circuit voltage and power conversion efficiency," *Polym. Mater. Sci. Eng.*, vol. 96, pp. 814–815, 2007.
[80] L. A. A. Pettersson, L. S. Roman, O. Ingana, and I. Introduction, "Modeling photocurrent action spectra of photovoltaic devices based on organic thin films," *J. Appl. Phys.*, vol. 86, no. 1, pp. 487–496, Jul. 1999.
[81] T. Stübinger and W. Brütting, "Exciton diffusion and optical interference in organic donor–acceptor photovoltaic cells," *J. Appl. Phys.*, vol. 90, no. 7, p. 3632, Oct. 2001.
[82] H. Hänsel *et al.*, "Optical and electronic contributions in double-heterojunction organic thin-film solar cells," *Adv. Mater.*, vol. 15 no. 24, pp. 2056–2060, Dec. 2003.
[83] B. O'Regan and M. Grätzel, "A low-cost, high-efficiency solar cell based on dye-sensitized colloidal TiO_2 films," *Nature*, vol. 353, pp. 737–740, 1991.
[84] U. Bach *et al.*, "Solid-state dye-sensitized mesoporous TiO_2 solar cells with high photon-to-electron conversion efficiencies," *Nature*, vol. 395, pp. 583–585, 1998.
[85] A. C. Arango *et al*, "Efficient titanium oxide/conjugated polymer photovoltaics for solar energy conversion," *Adv. Mater.*, vol. 12, no.22, pp. 1689–1692, Dec. 2000.
[86] A. J. Breeze, Z. Schlesinger, S. A. Carter, and P. J. Brock, "Charge transport in TiO_2/MEH−PPV polymer photovoltaics," *Phys. Rev. B*, vol. 64, no. 12, pp. 125205-1–125205-9, 2001.
[87] B. P. A. Van Hal *et al.*, "Photoinduced electron transfer and photovoltaic of a MDMO-PPV:TiO2 bulk-heterojunction," *Adv. Mater.*, vol. 15, no. 2, pp. 118–121, Jan. 2003.
[88] K. Lee, Y. Chang, and J. Y. Kim, "Optical spectroscopic characterization of plasma-polymerized thin films," *Thin Solid Films*, vol. 423, no. 2, pp. 131–135, Jan. 2003.
[89] A. Roy *et al.*, "Titanium suboxide as an optical spacer in polymer solar cells," *Appl. Phys. Lett.*, vol. 95, no. 1, pp. 013302-1–013302-3, Jul. 2009.
[90] C. J. Brabec, S. E. Shaheen, C. Winder, N. S. Saricifci, and P. Denk, "Effect of LiF/metal electrodes on the performance of plastic solar cells," *Appl. Phys. Lett.*, vol. 80, no. 7, pp. 1288, Feb. 2001.
[91] B. G. Streetman and B. Sanjay, *Solid State electronic Devices*, 5th ed. Englewood Cliffs, NJ, USA: Prentice-Hall, 2000, pp. 524.
[92] T. J. Savenjie, "Exciton solar cells," in *Organic Solar Cells*. Delft, The Netherlands: Delft Univ. Technol.
[93] A. F. Nogueira *et al.*, "Charge recombination in conjugated polymer/fullerene blended films studied by transient absorption spectroscopy," *J. Phys. Chem. B.*, vol. 107, no. 7, pp. 1567–1573, 2003.
[94] C. Honsberg and S. Bowden. (Jun. 1, 2013). *Absorption Depth*. [Online]. Available: http://pveducation.org/pvcdrom/pn-junction/absorption-depth
[95] A. J. Moulé, J. B. Bonekamp, and K. Meerholz, "The effect of active layer thickness and composition on the performance of bulk-heterojunction solar cells," *J. Appl. Phys.*, vol. 100, no. 9, pp. 094503-1–094503-7, Nov. 2006.
[96] Z. Zhao, L. Rice, H. Efstathiadis, and P. Haldar, "Thickness dependent effects of thermal annealing and solvent vapor treatment of poly(3-hexylthiophene) and fullerene bulk heterojunction photovoltaics," *Proc. Mater. Res. Soc.*, vol. 1123, pp. 1–8, 2009.
[97] G. Li *et al.*, "High-efficiency solution processable polymer photovoltaic cells by self-organization of polymer blends," *Nat. Mater.*, vol. 4, no. 11, pp. 864–868, 2005.
[98] S. E. Shaheen *et al.*, "2.5% efficient organic plastic solar cells," *Appl. Phys. Lett.*, vol. 78, no. 6, pp. 841–843, Feb. 2001.
[99] H. Hoppe *et al.*, "Nanoscale morphology of conjugated polymer/fullerene based bulk-heterojunction solar cells," *Adv. Functional Mater.*, vol. 14, no. 10, pp 1005–1011, Oct. 2004.
[100] J. K. Lee *et al.*, "Processing additives for improved efficiency from bulk heterojunction solar cells.," *J. Amer. Chem. Soc.*, vol. 130, no. 11, pp. 3619–3623, 2008.
[101] B. R. Aïch, J. Lu, S. Beaupré, M. Leclerc, and Y. Tao, "Control of the active layer nanomorphology by using co-additives towards high-performance bulk heterojunction solar cells," *Org. Electron.*, vol. 13, no. 9, pp. 1736–1741, 2012.
[102] V. Shrotriya, J. Ouyang, R. J. Tseng, G. Li, and Y. Yang, "Absorption spectra modification in poly(3-hexylthiophene): Methanofullerene blend thin films," *Chem. Phys. Lett.*, vol. 411, no. 1–3, pp. 138–143, Aug. 2005.

[103] K. M. Coakley and M. D. McGehee, "Conjugated polymer photovoltaic cells," *Chem. Mater.*, vol. 16, no. 23, pp. 4533–4542, 2004.
[104] F. Yang, M. Shtein, and S. R. Forrest, "Controlled growth of amolecular bulk heterojunction photovoltaic cell," *Nat. Mater.*, vol. 4, pp. 37–41, 2005.
[105] D. Chirvase, J. Parisi, J. C. Hummelen, and V. Dyakonov, "Influence of nanomorphology on the photovoltaic action of polymer–fullerene composites," *Nanotechnol.*, vol. 15, no. 9, pp. 1317, Aug. 2004.
[106] S. Cho *et al.*, "A thermally stable semiconducting polymer," *Adv. Mater.*, vol. 22, no. 11, pp. 1253-7, Mar. 2010.
[107] ASTM G-173-03, Terrestrial Reference Spectra for Photovoltaic Performance Evaluation, Amer. Soc. Testing Mater. (ASTM) Int., West Conshohoken, PA, USA.
[108] C. Society, "Random polyfluorene co-polymers designed for a better optical absorption coverage of the visible region of the electromagnetic spectrum," *Bull. Chem. Soc. Ethiop.*, vol. 28, no. 1, pp. 121–130, 2014.
[109] C. H. Peters *et al.*, "High efficiency polymer solar cells with long operating lifetimes," *Adv. Energy Mater.*, vol. 1, no. 4, pp. 491–494, Jul. 2011.
[110] D. H. Wang *et al.*, "Enhancement of donor-acceptor polymer bulk heterojunction solar cell power conversion efficiencies by addition of Au nanoparticles," *Angewandte Chemie Int. Ed. Engl.*, vol. 50, no. 24, pp. 5519–5523, Jun. 2011.
[111] S.-W. Baek *et al.*, "Plasmonic forward scattering effect in organic solar cells: A powerful optical engineering method," *Sci. Rep.*, vol. 3, no. 1726, pp. 1–7, 2013.
[112] S.-S. Kim, S.-I. Na, J. Jo, D.-Y. Kim, and Y.-C. Nah, "Plasmon enhanced performance of organic solar cells using electrodeposited Ag nanoparticles," *Appl. Phys. Lett.*, vol. 93, no. 7, pp. 073307-1–073307-3, Aug. 2008.
[113] J.-L. Wu *et al.*, "Surface plasmonic effects of metallic nanoparticles on the performance of polymer bulk heterojunction solar cells," *ACS Nano*, vol. 5, no. 2, pp. 959–967, 2011.
[114] J. Zhu *et al.*, "Plasmonic effects for light concentration in organic photovoltaic thin films induced by hexagonal periodic metallic nanospheres," *Appl. Phys. Lett.*, vol. 98, no. 15, pp. 151110-1–1151110-3, Apr. 2011.
[115] L. Lu, Z. Luo, T. Xu, and L. Yu, "Cooperative plasmonic effect of Ag and Au nanoparticles on enhancing performance of polymer solar cells," *Nano Lett.*, vol. 13, no. 1, pp. 59–64, 2013.
[116] H. Atwater and A. Polman, "Plasmonics for improved photovoltaic devices," *Nat. Mater.*, vol. 9, no. 3, pp. 205–213, Mar. 2010.
[117] V. E. Ferry, J. N. Munday, and H. A. Atwater, "Design considerations for plasmonic photovoltaics," *Adv. Mater.*, vol. 22, no. 43, pp. 4794–4808, 2010.
[118] M.-G. Kang, T. Xu, H. J. Park, X. Luo, and L. J. Guo, "Efficiency enhancement of organic solar cells using transparent plasmonic Ag nanowire electrodes," *Adv. Mater.*, vol. 22, no. 39, pp. 4378–4383, Oct. 2010.
[119] W. Bai *et al.*, "Broadband short-range surface plasmon structures for absorption enhancement in organic photovoltaics," *Opt. Exp.*, vol. 18, no. S4, pp. A620–A630, Nov. 2010.
[120] B. Zeng, Q. Gan, Z. H. Kafafi, and F. J. Bartoli, "Polymeric photovoltaics with various metallic plasmonic nanostructures," *J. Appl. Phys.*, vol. 113, no. 6, p. 063109, Feb. 2013.
[121] J. A. Christians, R. C. M. Fung, and P. V. Kamat, "An inorganic hole conductor for organo-lead halide perovskite solar cells. Improved hole conductivity with copper iodide," *J. Amer. Chem. Soc.*, vol. 136, no. 2, pp. 758–764, 2014.
[122] "Heliatek consolidates its technology leadership by establishing a new world record for organic solar technology with a cell efficiency of 12%," Jun. 14, 2014. [Online]. Available: http://www.heliatek.com
[123] M. Peach, "Heliatek achieves 12% organic solar cell efficiency," Jun. 14, 2014. [Online]. Available: http://optics.org/news/4/1/36